

AFIT/GA/ENY/97D-02

APPLYING FLYWHEEL ENERGY STORAGE TO SOLAR ELECTRIC ORBITAL
TRANSFERS

THESIS

Presented to the Faculty of the Graduate School of Engineering
of the Air Force Institute of Technology

Air University

In Partial Fulfillment of the
Requirements for the Degree of
Master of Science

Mark William Marasch, B.S.

Captain, USAF

December, 1997

Approved for public release; distribution unlimited

APPLYING FLYWHEEL ENERGY STORAGE TO SOLAR ELECTRIC ORBITAL
TRANSFERS

Mark William Marasch, B.S.
Captain, USAF

Approved:

Dr. William E. Wiesel (Chairman)

date

Lt Col Stuart C. Kramer

date

Maj Jeffrey S. Turcotte

date

Acknowledgments

First, I must thank Dr. Christopher D. Hall, my thesis advisor. Dr. Hall did a great job of pointing me in the right direction on this project. After leaving AFIT for Virginia Tech, Dr. Hall has shown continued dedication to supporting these efforts. His advice on matters both technical and literary are highly valued.

I would also like to thank Dr. William E. Wiesel for playing the role of my "local" thesis advisor after Dr. Hall's move. Dr. Wiesel contributed much to the direction of this thesis, and has been a source for good technical advice.

Most of all, I must thank my wife, Catherine D. Marasch, for her love, patience, and support. It has been a journey that would have been much more difficult without her. Finally, I must not forget to thank my canine study partner, Wolfgang, who deserves credit for his moral support.

Mark W. Marasch

Table of Contents

Acknowledgments	iii
Table of Contents.....	iv
List of Figures	vii
List of Tables	ix
List of Symbols.....	x
Abstract.....	xii
I. Introduction	1
Problem Statement.....	2
Research Goal.....	3
Thesis Outline.....	3
II. Literature Review	5
Flywheel Energy Storage	5
Low Thrust Orbital Transfers and Solar Electric Propulsion	6
The Subjects Combined.....	7
III. Methodology	10
Geometry of the Earth's Shadow	10
CASE ONE: Circle-to-Circle Transfer Segments Without Shade Constraints	12

Case Two: Transfer Segments Without Energy Storage	17
Case Three: Low Levels of Energy Storage	20
Case Four: High Levels of Energy Storage.....	24
Case Five: A Final Orbital Transfer Segment Requiring Energy Storage	27
Summary.....	29
IV. Flywheel Energy Storage Used Strictly for Propulsion	30
Effects of a Mass Tradeoff.....	30
Effects of Other Variables	41
Concepts Applied to a LEO to GEO Transfer	48
Conclusions	54
V. Flywheel Energy Storage Baselined for On-Orbit Needs	55
Spacecraft With Minimum Requirements	55
Adding Additional Battery and Array Mass	59
Summary.....	65
VI. Summary, Conclusions, and Recommendations	66
Summary.....	66
Conclusions	66
Recommendations.....	68
APPENDIX A. Numerical Techniques Used For Integration	70
APPENDIX B Conversion to and From Canonical Units	72
BIBLIOGRAPHY	75

Vita78

List of Figures

Figure 1. Shadow Geometry	10
Figure 2. Simplified Shadow Geometry in the Ecliptic Plane	11
Figure 3. An Optimal Circle-to-Circle Transfer	12
Figure 4. Optimal Transfer Geometry in Polar Coordinates.....	14
Figure 5. Maximum Transfer Accomplished While in Sunlight	18
Figure 6. An Orbital Transfer Segment With a Low Level of Energy Storage	20
Figure 7. An Orbital Transfer Without a Coast Phase.....	25
Figure 8. Algorithm Used for Comparisons Based on a Mass Ratio at a Fixed Initial Altitude.	33
Figure 9. Trajectories For Different Flywheel to Array Mass Ratios	34
Figure 10. Control Angle Histories For Several Battery and Array Mass Ratios.....	35
Figure 11. Final Radius Versus Fraction of Mass Allocated for Flywheel Battery	36
Figure 12. Final Radius vs. Fraction of Balance Battery Mass Used for Battery, in Low Earth Orbit	38
Figure 13. Final Radius Versus Fraction of Balance Battery Mass Used for Battery, for a Higher Altitude	39
Figure 14. Final Radius Versus Fraction of Balance Battery Mass Used, for Reduced Useful Energy Density	40
Figure 15. Algorithm For Finding Break-even Beta vs. Altitude	42
Figure 16. Break-Even Values of Beta for Different Balance-Case Panel Masses	43

Figure 17. Break-Even Values of Beta for Several Different Sets of Engine Characteristics.....	45
Figure 18. Break-Even Beta Versus Alpha For Several Altitudes.....	46
Figure 19. β/α for Many Configurations and Altitudes.....	47
Figure 20. An Algorithm for Simulating a Large Orbital Transfer	49
Figure 21. Algorithm for Determining Appropriate Case	50
Figure 22. Radius Versus Time, For Two Spacecraft Configurations.....	51
Figure 23. Radius Versus Time For the First 15 Days	52
Figure 24. Spacecraft Mass Remaining With Respect to Radius Achieved.....	53
Figure 25. Radius Versus Time Comparison For Two Transfer Schemes	57
Figure 26. Radius Increase Ratios Versus Radius Comparison.....	58
Figure 27. Mass Versus Radius Comparison.....	59
Figure 28. Radius Versus Time for Two Extreme Configurations.....	61
Figure 29. Mass Remaining Versus Radius for Two Extreme Cases.....	62
Figure 30. Radius Versus Time With Intermediate Cases Added	63
Figure 31. Radius Ratio Versus Initial Radius With Intermediate Cases	63
Figure 32. Radius Ratio Versus Time With Intermediate Cases	64
Figure 33. Mass Versus Radius With Intermediate Cases.....	64

List of Tables

Table 1. Battery Characteristics [17:11]2

Table 2. Circle-to-Circle Boundary Value Problem 15

Table 3. Characteristics of Engines Simulated [21][1].....44

List of Symbols

a	acceleration
D	difference between collected energy and energy storage capacity
F	fraction of power applied to power available
G	excess energy
g_0	gravitational acceleration at the Earth's surface
m	mass
\dot{m}	mass flow rate
P_a	power applied to thruster
P_e	power available from solar array
\mathbf{P}	correction vector
r	distance between spacecraft and the Earth's center
r_\oplus	radius of the Earth
t	time
t_f	time of flight
T	thrust
u	radial component of velocity
v	transverse component of velocity
α	shadow geometry angle
ϕ	angle between thrust direction and local horizontal
γ	shadow half-angle
η	engine efficiency

λ_r	costate for radius
λ_u	costate for radial velocity component
λ_v	costate for transverse velocity component
μ	gravitational parameter
θ	angular measure of spacecraft position

Abstract

In this thesis, we investigate the application of flywheel energy storage to minimum-time, constant-thrust orbital maneuvers using electric propulsion. Techniques for solving several resulting boundary value problems are developed. Tradeoffs between solar array and flywheel battery masses are explored for single segment transfers and transfers requiring multiple segments. The effects of several parameters on these tradeoffs are examined. The utility of flywheel energy storage specifically for the use of the solar electric propulsion system is examined. It is found that when flywheel energy storage is used in these scenarios, transit times are typically increased, but significant propellant mass savings can be realized. The utility of flywheel energy storage is examined for cases where the spacecraft has minimum requirements for energy storage. It is found that when energy storage is present, it is advantageous to make use of it in orbital transfers. It is found that when additional mass is allowed, adding flywheel battery mass may give diminishing returns in terms of propellant mass savings, while significantly increasing transit time.

APPLYING FLYWHEEL ENERGY STORAGE TO SOLAR ELECTRIC ORBITAL TRANSFERS

I. Introduction

Solar electric propulsion (SEP) is a topic that receives much attention in the search for economical means to move spacecraft to high Earth orbits and to explore the solar system. Solar electric propulsion is a term used to describe any system providing thrust by utilizing electrical power generated by the collection of solar energy. When SEP is applied to orbital transfers in the near-Earth environment, the Earth's shadow becomes a concern. Typically, it is assumed that a spacecraft has to coast when it is in eclipse. The conventional battery mass necessary to permit continuous thrust through eclipse is excessively large [4:1217]. This barrier may be overcome by the use of flywheel energy storage.

In the generic sense, flywheels can be found in common mechanical systems as a means for storing mechanical energy. In this thesis we discuss the use of flywheel batteries used to store electric energy. Properties that make flywheel batteries especially useful for space use include their energy density, cycle life, and efficiency. Values comparing nickel-cadmium, nickel-hydrogen, and flywheel batteries can be found in Table 1. Note that flywheel batteries are capable of outperforming these common electrochemical batteries in both cycle life and energy density [17:11]. Flywheel batteries have a high effi-

ciency of 80 to 90 %, compared to nickel-hydrogen battery efficiencies of 60 to 80 % [19:8].

Table 1. Battery Characteristics [17:11]

Battery Type	Energy Density (Whr/kg)	Cycle Life
Nickel-Cadmium	10-30	20,000
Nickel-Hydrogen	20-35	40,000
Flywheel	25-65	60,000

Other important issues include temperature sensitivity and depth of discharge. Due to their mechanical nature, flywheels are much less sensitive to temperature variations than chemical batteries are. Reducing the need for insulation and temperature regulation reduces spacecraft mass and complexity. Chemical batteries have a limited depth of discharge and cycle life. The achievable depth of discharge of a flywheel battery system is normally limited only by the electronic portions of the system [19:19]. A flywheel's material properties are the limiting factor in its cycle life [15:589-590].

Because flywheels incorporate spinning masses, they can be used for attitude control. Using a system of four or more flywheels, energy storage and attitude control can be performed simultaneously. Using flywheel batteries for both energy storage and primary attitude control can achieve further mass savings [16,590].

Problem Statement

It is easy to see how adding energy storage to a spacecraft's solar electric propulsion system can decrease orbital transfer times by allowing thrusters to operate during eclipse. When simplifying assumptions are made about low-thrust transfers, it is difficult to comprehend how a spacecraft could accomplish this feat without significantly increas-

ing spacecraft mass. Fitzgerald used such methods, and came to the conclusion that energy storage for this purpose is not feasible [11]. Combining the use of true optimal transfers with the high energy density of flywheel batteries may overcome this obstacle. The conditions under which flywheel energy storage provides true benefits must be determined.

Research Goal

The goal of this research is to provide insight into the conditions under which an energy storage scheme would be beneficial for savings of time, propellant mass, or both. New techniques must be developed to simulate optimal transfers with shade, power, and storage constraints. The effects of altitude, propulsion system choice, panel specific power, and flywheel battery specific energy are examined for single transfer segments. Results of these tradeoffs are applied to complete simulated large-scale transfers that compare different levels of flywheel energy storage use.

Thesis Outline

Chapter Two is the literature review, which provides an overview of the work already accomplished in this and related topics. Chapter Three develops the methodology, discussing the processes used for solving several boundary-value problems. When solved, the results of these problems describe optimal transfer segments. In Chapter Four, we discuss the tradeoffs involved in using of energy storage specifically for the purpose of propulsion. We consider single segment tradeoffs, and simulate some large-scale transfers. In Chapter Five, we consider a large-scale transfer for a spacecraft that has a minimum requirement for energy storage based on its on-orbit mission. When

allowed a fixed increase in the combined mass of the array and battery, we determine which combination gives the best results.

II. Literature Review

In this thesis, we combine the subjects of solar electric propulsion (SEP) and flywheel energy storage. In this chapter, we provide an overview of the literature currently available on these subjects. While much is available on each individual subject, the combination is rarely found in astronomical literature. The literature which is available covering the combination of these subjects does not further combine these subjects with that of optimal orbital transfers.

Flywheel Energy Storage

In recent years, flywheel energy storage (FES) systems have received increasing attention, because of high energy densities, high depth of discharge, and long lifespans. A number of applicable papers discussing future capabilities and applications of FES were presented at the 1997 National Aerospace and Electronics Conference (NAECON). In Reference [16], Pieronek, Decker, and Spector discuss the wide range of benefits that FES may provide for space-based applications. Christopher and Beach also discuss FES benefits in Reference [8], but move on to describe NASA's flywheel technology development program. In Reference [9], Edwards, Aldrich, Christopher, and Beach discuss a project to demonstrate FES on the International Space Station.

Most of the literature available on the combination of FES and propulsion is devoted to the subject of ground transportation. Through the combination of load-leveling and regenerative braking, ground vehicles can operate at higher efficiencies. Reference [10] discusses the application of such concepts for transit buses, while Refer-

ences [18] and [3] do so for automobiles and locomotives. Unfortunately, no sources were found combining FES with electric space propulsion.

Low Thrust Orbital Transfers and Solar Electric Propulsion

Because of the potential for solar electric propulsion to lower costs, increase payload ratios, and enable exploration, it receives a great deal of coverage in astronomical literature. The papers available on the topics of solar electric propulsion and low thrust orbital transfers range from purely theoretical work to the subject of actual projects that demonstrate the maturing technologies involved.

At the Air Force Institute of Technology (AFIT), alone, a great deal of theoretical literature is available on the related subjects of low-thrust and solar electric propulsion. In Reference [2] Alfano examined basic low-thrust orbital transfers. In Reference [7] Cass explored discontinuous transfers for solar electric spacecraft passing through the Earth's shadow. In Reference [15] McCann worked on the problem of optimal launch-time for discontinuous transfers. Thorne formulated methods that allow constant-thrust orbital transfers to be solved for a large variety of cases in References [23] and [24]. Outside of AFIT, many other sources are available in this field. Spencer and Culp discuss a process for designing large-scale continuous-thrust transfers in Reference [21]. Another work of interest is Reference [20], a journal article by Scheel and Conway, where some of the most current techniques used for solving orbital transfers involving many revolutions about the primary body are discussed.

Literature on planned projects involving practical applications of solar propulsion is readily available. Miller, Seaworth, Bell, and Cady discuss system level requirements

for a SEP system [14]. In Reference [4], Avila discusses parametric studies related to the Electric Insertion Transfer Experiment (ELITE) being developed cooperatively by Phillips Laboratory and TRW. In another Air Force project, Phillips Laboratory is working on the Integrated Solar Upper Stage (ISUS) Program, as discussed in Reference [12]. While this program involves solar thermal propulsion, rather than solar electric propulsion, some of the problems addressed are similar to those addressed by SEP systems.

The Subjects Combined

Though there is a wealth of information available in the subjects of flywheel energy storage, low-thrust transfers, and SEP, few sources dedicate any attention to the possibility of improving solar electric propulsion through the use of energy storage. No sources were found that combine FES and SEP. In most of the cases where energy storage is addressed, the concept is quickly dismissed. Avila is quick to point out that, if conventional battery systems are used, the mass required to run thrusters in eclipse is prohibitively large [4:1217]. Avila's views are backed-up by Fitzgerald, whose work is among a select few that directly address the issue of SEP and energy storage. Fitzgerald examines how adding batteries to a solar electric propulsion system can assist in decreasing the transit time to a higher Earth orbit in Reference [11], by allowing thrusters to be run in eclipse. Because this work does not use optimal transfers, assumes that thrusters are always operated at full capacity, and uses a conventional battery-type with a low specific energy, the results show that the advantage gained in terms of transit time is far outweighed by the increase in system mass.

Though the problem has been addressed in its most basic form, a more in-depth study is needed. When non-optimal transfers are used, it is a great deal more difficult to see where using energy storage can lead to an advantage, especially where energy storage is concerned. By examining this problem in terms of optimal transfers, a more accurate situation can be realized.

III. Methodology

In this thesis, we examine orbital transfers that take many revolutions to complete. In order to create situations where information about a transfer is easily obtained and problems involving numerical integration are easily solved, we choose to break large transfers into single revolution segments. Each segment begins as the spacecraft leaves the Earth's shadow, and is described as an optimal, planar, constant-thrust, circle-to-circle transfer. If a spacecraft has no capacity to store energy for propulsion, each of these transfers must be completed when it returns to the Earth's shadow. When the spacecraft has some energy storage capacity, these transfer segments are allowed to continue into the Earth's shadow until the stored energy is exhausted. When a spacecraft has enough energy storage to continue thruster operation through the Earth's shadow, continuous transfers become possible. All of the trajectories in this thesis can be described by the same equations of motion, but each of the described cases presents a different boundary value problem to be solved.

In this chapter, we examine the schemes used to propagate optimal transfer segments and the techniques used to solve each scheme's boundary value problem. Most of the boundary value problems to be addressed involve the geometry of the Earth's shadow. Before we can move on to solve these boundary value problems, we must discuss the actual geometry of the Earth's shadow and the assumptions to be made.

Geometry of the Earth's Shadow

The true structure of the Earth's shadow involves an umbra and a penumbra. These cones of shadow are the result of the Sun not being a point-source of light. Figure

1 illustrates the geometry of this situation. The penumbra is an outward-opening cone of partial shadow, while the umbra is a closed cone of complete shadow. When a satellite enters the penumbra, the edge of the Sun's disk is obscured by the Earth's horizon. When the umbra is reached, the Sun has "set" completely. The penumbra is a region that sees a gradient of intensity. At the outer edge of the penumbra, a satellite receives 100% of the sunlight available in Earth's orbit. As the satellite approaches the umbra, less of the Sun is seen, until the Sun is completely obscured, and the umbra has been reached.

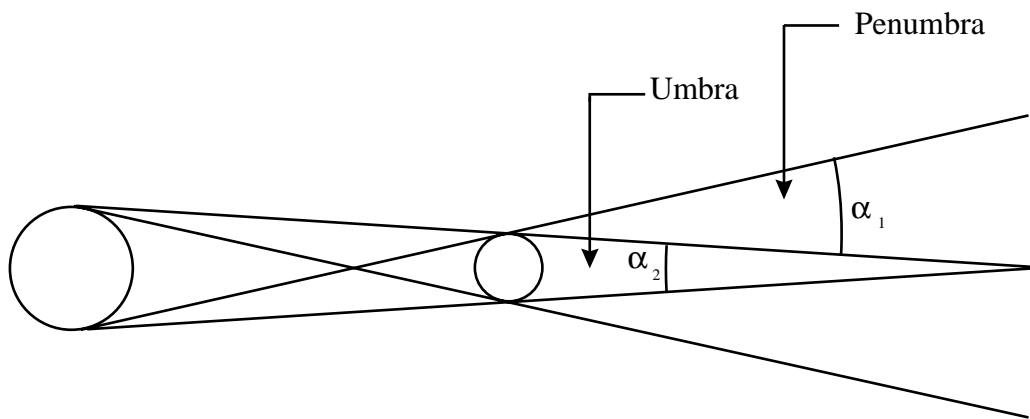


Figure 1. Shadow Geometry

The Earth is far enough from the Sun that we can approximate the angles marked α_1 and α_2 in Figure 1 as being identical to each other. They are approximated as the angular size of the Sun as seen from Earth's orbit, $\alpha = 0.00931$ radians [6:92]. This angle is small enough that shadow calculations are often made without taking it into consideration, such as in Reference [13]. When this assumption is applied, the Sun is treated as a point-source of light, and the Earth's shadow takes on the shape of a cone. The angle of this cone, α , is small enough to approximate it as a cylinder in the near-Earth environment.

In this thesis, all of the orbital transfers to be modeled are planar and in the ecliptic plane. This has the effect of maximizing time in eclipse for any orbital radius, providing the worst possible scenario for solar electric propulsion. The problem is now planar, and the Earth's shadow is found between two parallel lines, as shown in Figure 2. Using this geometry, the angular portion of a circular orbit spent in shade is 2γ , where

$$\gamma = \sin^{-1}\left(\frac{r_{\oplus}}{r}\right) \quad (1)$$

r_{\oplus} is the Earth's radius, and r is the radius of the orbit.

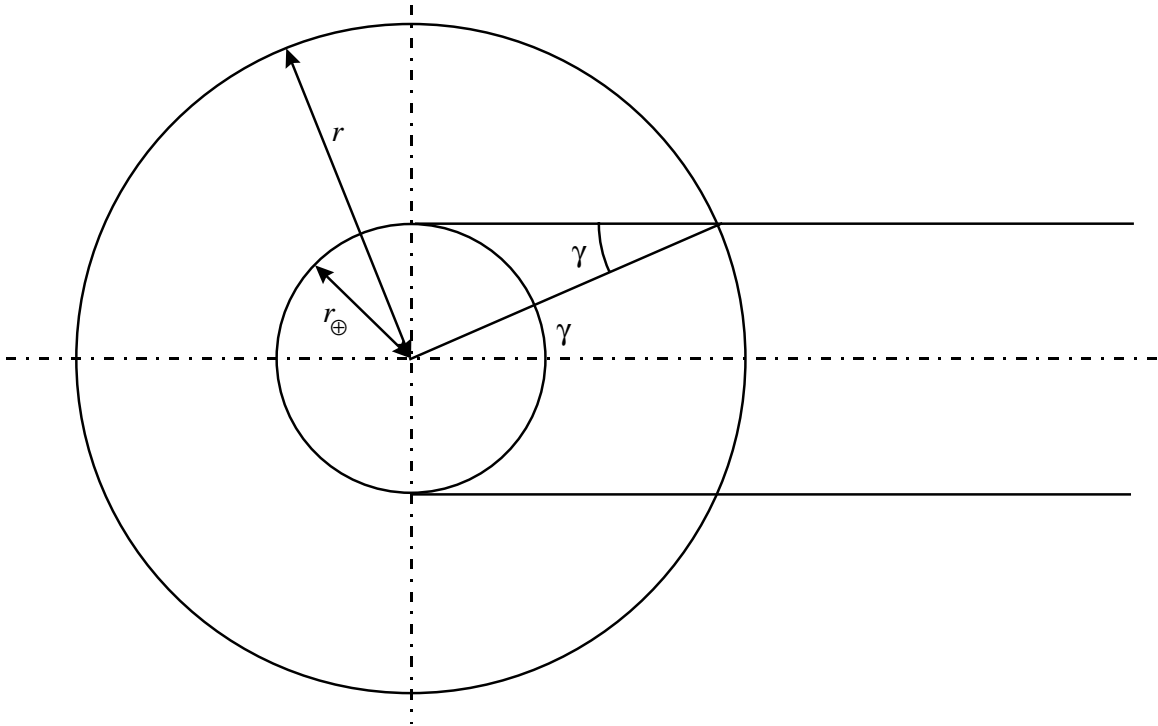


Figure 2. Simplified Shadow Geometry in the Ecliptic Plane

CASE ONE: Circle-to-Circle Transfer Segments Without Shade Constraints

When a transfer is small enough that it can be accomplished without entering the Earth's shadow, Case One is applicable. Figure 3 illustrates the concept of such a transfer, with dashed lines indicating the Earth's shadow, concentric circles depicting two circular orbits, and an arc connecting them representing a transfer between the two.

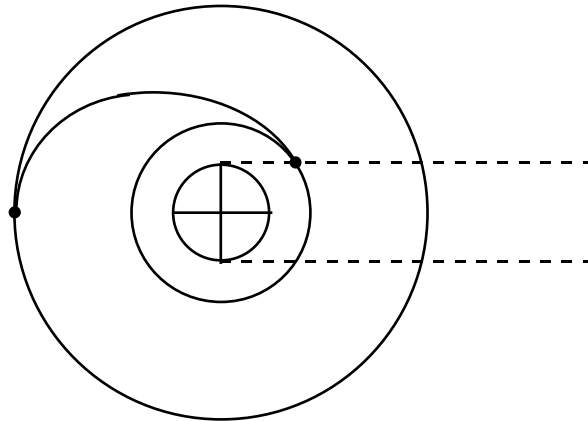


Figure 3. An Optimal Circle-to-Circle Transfer

In this thesis, this case does not receive heavy usage, but it is an important starting point for the work to be done. The technique for solving this case is developed in its entirety in Reference [23], where the equations of motion are developed in the following form:

$$\begin{aligned}
\dot{r} &= u \\
\dot{u} &= \frac{v^2}{r} - \frac{\mu}{r^2} + a(t) \sin \phi \\
\dot{v} &= -\frac{uv}{r} + a(t) \cos \phi \\
\dot{\lambda}_r &= -\lambda_u \left(-\frac{v^2}{r^2} + 2\frac{\mu}{r^3} \right) - \lambda_v \frac{uv}{r^2} \\
\dot{\lambda}_u &= \lambda_r + \lambda_v \frac{v}{r} \\
\dot{\lambda}_v &= -\lambda_u \frac{2v}{r} + \lambda_v \frac{u}{r} \\
a(t) &= \frac{T}{m(0) - \dot{m}t} \\
\phi &= \tan^{-1} \left(\frac{\lambda_u}{\lambda_v} \right)
\end{aligned} \tag{2}$$

These equations describe minimum-time, constant-thrust, planar orbital transfers in polar coordinates. For this case, the propulsion system runs at its full capacity, the thrust magnitude, T , and the mass flow rate, \dot{m} , are known. The variable r is the spacecraft's distance from the center of the primary body, u is the radial component of velocity, and v is the transverse component of velocity. Figure 4 illustrates the geometry of this problem. The variables λ_r , λ_u , and λ_v are the costates correlating to radius, radial velocity, and transverse velocity. $a(t)$ is the scalar acceleration magnitude of the spacecraft as a function of time, and ϕ is the angle between local horizontal and the thrust vector: $\phi = \tan^{-1}(\lambda_u/\lambda_v)$ [23].

Each transfer segment described by these equations uses a fixed thrust magnitude, and achieves a transfer in minimum time by continuously varying ϕ , the direction in which thrust is applied. For a constant-thrust transfer, one that minimizes time in transit also minimizes the propellant used [23].

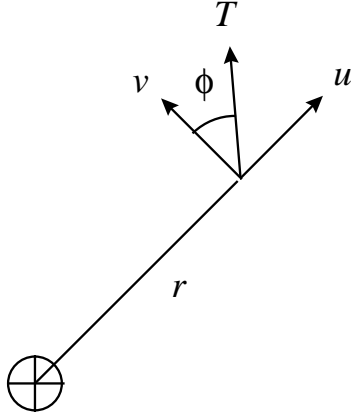


Figure 4. Optimal Transfer Geometry in Polar Coordinates

For the circle-to-circle problem, the known initial conditions are $r(0)$, $u(0)$, and $v(0)$. The desired final conditions are the given value of $r(t_f)$ and the values of $u(t_f)$ and $v(t_f)$ necessary to establish a circular orbit:

$$\begin{aligned} u(t_f) &= 0 \\ v(t_f) &= \sqrt{\frac{\mu}{r(t_f)}} \end{aligned} \quad (3)$$

In order to solve this problem, we must find the initial costates and the time of flight, t_f [23].

To assist in coding, this problem is generalized by switching to a system of canonical units as described by References [5] and [23]. Such a system of canonical units uses the initial circular orbit as a reference. The canonical distance unit (DU) is chosen to be the radius of the initial orbit, and the time unit (TU) is the period of time in which the spacecraft traces an arc one DU in length in its circular orbit. The convention for canonical units presented in Reference [13] uses the convention where one mass unit (MU) is equivalent to the mass of the primary body. Because the spacecraft mass is small in com-

parison to the mass of the Earth, the equations of motion can be decoupled without any noticeable consequences. Because of this decoupling, we can choose any system of units we wish to represent spacecraft mass. In this thesis, we use the convention where the spacecraft initial mass is one MU. This is the same convention used by Reference [23]. Regardless of the mass convention used, the gravitational parameter will satisfy $\mu = 1 \text{ DU}^3/\text{TU}^2$ [5:40-43]. All integrations propagated in this thesis are performed in canonical units. The methods that are used to convert values to and from canonical units are described in detail in Appendix B.

Using canonical units, we have the boundary value problem shown in Table 2. As shown, $\lambda_r(0)$ can be normalized, but the initial values of the other two costates are still unknown. The final values of the costates have been omitted, as they are not a concern.

Table 2. Circle-to-Circle Boundary Value Problem

Initial Conditions (Canonical Units)	Final Conditions (Canonical Units)
$r(0) = 1$	$r(t_f) = r(t_f)$
$u(0) = 0$	$u(t_f) = 0$
$v(0) = 1$	$v(t_f) = (1/r(t_f))^{1/2}$
$\lambda_r(0) = 1$	
$\lambda_u(0) = ?$	$t_f = ?$
$\lambda_v(0) = ?$	

Because there are three final conditions to be satisfied, and three unknown values, this problem can be solved. However, the equations of motion are highly nonlinear, and no closed-form solutions exist. The problem can be solved using an iterative process, such as a Newton method. To begin, a first approximation is made for the values of t_f , $\lambda_u(0)$,

and $\lambda_v(0)$. Then the equations of motion (Equations 2) are integrated for the period of time t_f . In all likely cases, the desired final conditions are not met on this first try. So, a Jacobian is created using a finite difference method, and changes to the three values can be made as:

$$\begin{bmatrix} \Delta t_f \\ \Delta \lambda_u(0) \\ \Delta \lambda_v(0) \end{bmatrix} = \begin{bmatrix} \frac{\partial r(t_f)}{\partial t_f} & \frac{\partial r(t_f)}{\partial \lambda_u(0)} & \frac{\partial r(t_f)}{\partial \lambda_v(0)} \\ \frac{\partial u(t_f)}{\partial t_f} & \frac{\partial u(t_f)}{\partial \lambda_u(0)} & \frac{\partial u(t_f)}{\partial \lambda_v(0)} \\ \frac{\partial v(t_f)}{\partial t_f} & \frac{\partial v(t_f)}{\partial \lambda_u(0)} & \frac{\partial v(t_f)}{\partial \lambda_v(0)} \end{bmatrix}^{-1} \begin{bmatrix} \Delta r(t_f) \\ \Delta u(t_f) \\ \Delta v(t_f) \end{bmatrix} \quad (4)$$

where $\Delta r(t_f)$, $\Delta u(t_f)$, and $\Delta v(t_f)$ are the differences between the current final values and the desired final values. If we call this change vector $\Delta \mathbf{P}$, a step-limiting procedure of the form

$$\Delta \mathbf{P}' = \frac{\Delta \mathbf{P}}{1 + \|\Delta \mathbf{P}\|} \quad (5)$$

is used to improve convergence by reducing the magnitude of large change values. $\Delta \mathbf{P}'$ is used to alter the approximations for t_f , λ_u , and λ_v . If reasonable first approximations are made for t_f , λ_u , and λ_v , repeated Newton iterations converge to the correct costates and time of flight [23:4-21]. Integration of the equations of motion with these values describes the desired trajectory [23].

Reference [23] discusses the initialization of this problem in great detail. Among Thorne's achievements was the formulation of first approximations that lead to converging results for a wide variety of cases. For most electric propulsion devices the

approximations based on low-thrust are adequate. These first approximate values are calculated as [23][6:15]:

$$\begin{aligned}\lambda_u &= 0 \\ \lambda_v &= 1 \\ t_f &= \frac{\sqrt{\mu}}{a(0)} \left[\frac{1}{\sqrt{r(0)}} - \frac{1}{\sqrt{r(t_f)}} \right]\end{aligned}\tag{6}$$

In this section, we discussed the process used to solve the basic circle-to-circle problem. Most of the transfer segments in this thesis have additional constraints that need to be addressed, and change the boundary problems that need to be solved. The basic approach used in this first case are repeated, but the details of each boundary value problem are quite different.

Case Two: Transfer Segments Without Energy Storage

For the second case, no energy storage is used and we wish to maximize the radius increase achieved during one period of sunlight. Integration can be carried out using the same equations of motion used by Case One, but the boundary value problem to be solved has changed. Because we are using minimum-time, constant-thrust transfers, we achieve the maximum value of $r(t_f)$ by utilizing the maximum useful value of t_f that gives a circle-to-circle transfer meeting the constraints. As illustrated in Figure 5, this transfer is maximized when the entire period spent in sunlight is used to complete the transfer. Note that the transfer is shown to begin just as the spacecraft exits the Earth's shadow, and ends just as it enters eclipse again. When a series of these maneuvers is used to create a large-scale orbital transfer, the spacecraft coasts along its new circular orbit until it leaves the Earth's shadow again. At this point, it begins the next maneuver.

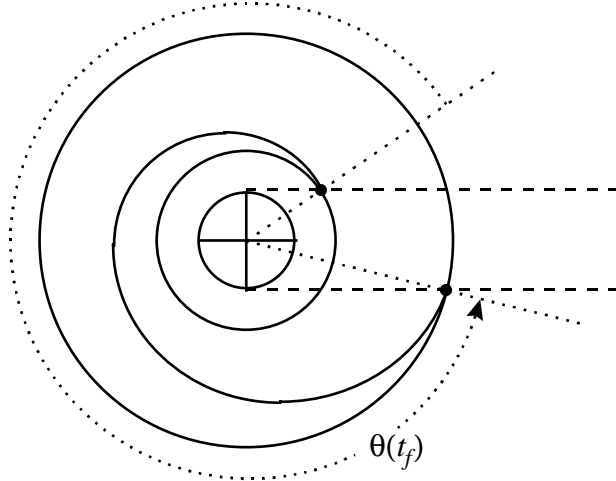


Figure 5. Maximum Transfer Accomplished While in Sunlight

In order for the transfer segment to end just as the spacecraft enters eclipse, Case One's $r(t_f)$ requirement is replaced by the angle requirement:

$$\theta(t_f) = 2\pi - \sin^{-1}\left(\frac{r_{\oplus}}{r(0)}\right) - \sin^{-1}\left(\frac{r_{\oplus}}{r(t_f)}\right) \quad (7)$$

where $\theta(t_f)$ is the angle swept out by the spacecraft in the transfer segment. Now, the spacecraft's angular position needs to be tracked, so we add $\dot{\theta} = v / r$ to the equations of motion.

By approximating the value of $r(t_f)$, we can solve the boundary value problem of Case One, and use a secant method to find the value of $r(t_f)$ that meets the angle requirement. However, this process encounters problems. Nested iterative processes require excessively high integration accuracy, causing them to be inefficient and less likely to converge.

Instead of using such an inefficient method, we choose to solve the boundary value problem directly. By replacing each occurrence of $r(t_f)$ in Equation (4) with $\theta(t_f)$, we create Newton steps that lead to solving this problem directly.

$$\begin{bmatrix} \Delta t_f \\ \Delta \lambda_u(0) \\ \Delta \lambda_v(0) \end{bmatrix} = \begin{bmatrix} \frac{\partial \theta(t_f)}{\partial t_f} & \frac{\partial \theta(t_f)}{\partial \lambda_u(0)} & \frac{\partial \theta(t_f)}{\partial \lambda_v(0)} \\ \frac{\partial u(t_f)}{\partial t_f} & \frac{\partial u(t_f)}{\partial \lambda_u(0)} & \frac{\partial u(t_f)}{\partial \lambda_v(0)} \\ \frac{\partial v(t_f)}{\partial t_f} & \frac{\partial v(t_f)}{\partial \lambda_u(0)} & \frac{\partial v(t_f)}{\partial \lambda_v(0)} \end{bmatrix}^{-1} \begin{bmatrix} \Delta \theta(t_f) \\ \Delta u(t_f) \\ \Delta v(t_f) \end{bmatrix} \quad (8)$$

As in each case presented, step-limiting is used, following the form of Equation (5). The remaining detail is to initialize approximations for Δt_f , $\Delta \lambda_u$, and $\Delta \lambda_v$ that are close enough for the problem to converge.

Because electric propulsion is being used, we use a low-thrust assumption. Because of the use of low thrust, the initial thrust vector is nearly tangential to the initial circular orbit. Under this condition $\phi = 0$, and because

$$\tan \phi = \frac{\lambda_u}{\lambda_v} \quad (9)$$

a reasonable first approximation is that:

$$\begin{aligned} \lambda_u &= 0 \\ \lambda_v &= 1 \end{aligned} \quad (10)$$

For the first approximation of t_f , we also use the low-thrust assumption. Because we know that the spacecraft does not have enough thrust to make any substantial changes to its initial circular orbit, we assume that the transfer segment is nearly circular. The time of flight for a circular orbit is:

$$t_f = 2\pi \sqrt{\frac{r^3}{\mu}} \quad (11)$$

Subtracting the time spent in the Earth's shadow in this circular approximation, we get:

$$t_f = 2 \left[\pi - \sin^{-1} \left(\frac{r_\theta}{r(0)} \right) \right] \sqrt{\frac{r^3}{\mu}} \quad (12)$$

So, now we have the approximations we need to begin the process of solving this case through the use of Newton iteration. Numerical experience shows that these guesses are adequate to obtain convergence.

Case Three: Low Levels of Energy Storage

A spacecraft may have some degree of energy storage, but not enough to continue thruster operation through the entire eclipse. Under these circumstances, we perform a circle-to-circle transfer as illustrated in Figure 6.

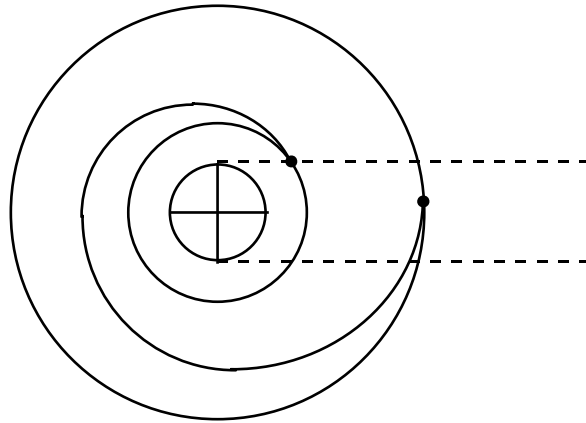


Figure 6. An Orbital Transfer Segment With a Low Level of Energy Storage

Here, the spacecraft begins a transfer segment as it leaves the Earth's shadow and completes a circle-to-circle transfer just as the stored energy is depleted. When a series of these maneuvers is combined to create a large-scale transfer, the spacecraft coasts in its new circular orbit until it leaves the Earth's shadow. Then, it begins another maneuver.

With the presence of energy storage, budgeting energy becomes a concern. If all of the power received by the solar array is sent directly to the thrusters, there is no stored energy to use in eclipse. To get the most out of this situation, it is best to channel just enough power to the flywheel batteries to give them a full charge at the moment the spacecraft enters eclipse. The remaining power can be used to run the thrusters in sunlight. Because we are using equations of motion designed for constant thrust, we continue to run the thrusters at the same power level in eclipse, until the energy supply is exhausted.

In order to achieve an energy balance, the engines are not used at full power. In order to have a manageable model of thrust and mass flow, a simplifying assumption is made. Thrust and mass flow are assumed to be directly proportional to the power supplied to the engines. This assumption is not very good if the thrusters being modeled use nozzles. Nozzles are designed to provide maximum efficiency for a fixed combustion chamber pressure and temperature. They do not deliver design efficiencies at off-design conditions. So, this assumption is not valid for electrothermal thrusters such as arcjets and resistojets, where heated gasses provide thrust as they expand and are accelerated by a nozzle. For electrostatic and magnetoplasmadynamic thrusters this model can be a valid approximation. For electrostatic thrusters, the potential drop across the accelerating screens can be kept constant, and the flow of reaction mass to be ionized and accelerated can be scaled for different power levels. Because the exit velocities are not changed, specific impulse does not change, leading to linear relationships between thrust, mass flow rate, and power. Similar arguments can be applied to magnetoplasmadynamic or Hall-effect devices. These assumptions should also be valid for pulsed devices. In

pulsed devices, different power levels applied can be accommodated by varying the length of time between pulses. Using these approximations for mass flow rate and thrust, we are able to continue examination of this problem.

The spacecraft has a fixed value of power from the solar array, P_e , and we have to find the level of power that is actually applied to the thrusters, P_a . We choose to use a power fraction, F , in solving this problem, where:

$$F = \frac{P_a}{P_e} \quad (13)$$

In order to solve this problem, we need to find t_f , λ_u , λ_v , and F . Because this spacecraft is to perform a circle-to-circle transfer, $u(t_f)$ and $v(t_f)$ must meet the requirements listed in Equations (3). The need to budget energy results in two new constraints. The first is the requirement that the energy used is exactly the energy that is collected by the solar array (assuming 100% storage efficiency).

$$P_a t_f = P_e t_{sun} \quad (14)$$

In this equation, t_{sun} is the period of time spent in sunlight. This condition must be met, as the spacecraft can not use more energy than its array collects. Also, if any of the collected energy is not utilized, the system performance is suboptimal. In order to simplify the problem, we define G as:

$$G = P_e t_{sun} - P_a t_f \quad (15)$$

A positive value of G represents excess energy that is not used. A negative value of G is an energy deficit. To satisfy Equation 14, the value of G should be zero. The other constraint to be enforced is that the battery must be fully charged just as the spacecraft enters the Earth's shadow, meaning:

$$m_f \beta = (P_e - P_a) t_{sun} \quad (16)$$

where m_f is the mass of the flywheel battery system, and β is the *usable* energy density.

If, for instance, we have 100 Whr/kg flywheel batteries designed for up to a 90% depth of discharge, $\beta = 90$ Whr/kg. We use D to represent the difference between battery charge and capacity:

$$D = (P_e - P_a) t_{sun} - m_f \beta \quad (17)$$

As with G , the solution must satisfy $D = 0$.

Now, we have a 4×4 problem. As in Case Two, we are not concerned about the final radius when solving the boundary value problem. Because we are using the minimum-time, constant thrust equations of motion, whatever value of $r(t_f)$ is obtained is the maximum that meets the constraints. One Newton step is calculated as:

$$\begin{bmatrix} \Delta t_f \\ \Delta \lambda_u(0) \\ \Delta \lambda_v(0) \\ \Delta F \end{bmatrix} = \begin{bmatrix} \frac{\partial D}{\partial t_f} & \frac{\partial D}{\partial \lambda_u(0)} & \frac{\partial D}{\partial \lambda_v(0)} & \frac{\partial D}{\partial F} \\ \frac{\partial u(t_f)}{\partial t_f} & \frac{\partial u(t_f)}{\partial \lambda_u(0)} & \frac{\partial u(t_f)}{\partial \lambda_v(0)} & \frac{\partial u(t_f)}{\partial F} \\ \frac{\partial v(t_f)}{\partial t_f} & \frac{\partial v(t_f)}{\partial \lambda_u(0)} & \frac{\partial v(t_f)}{\partial \lambda_v(0)} & \frac{\partial v(t_f)}{\partial F} \\ \frac{\partial G}{\partial t_f} & \frac{\partial G}{\partial \lambda_u(0)} & \frac{\partial G}{\partial \lambda_v(0)} & \frac{\partial G}{\partial F} \end{bmatrix}^{-1} \begin{bmatrix} \Delta D \\ \Delta u(t_f) \\ \Delta v(t_f) \\ \Delta G \end{bmatrix} \quad (18)$$

As we have done in the previous problems, we now need to initialize values of t_f , λ_u , λ_v , and F by finding reasonable approximations. Acceptable first approximations for λ_u and λ_v are unchanged from Case 2:

$$\begin{aligned} \lambda_u &= 0 \\ \lambda_v &= 1 \end{aligned} \quad (10)$$

In order to get a reasonable first approximation for F , we begin with the relationship that the time of flight is equal to the time spent in sunlight plus the time it takes to exhaust the stored energy:

$$t_f = t_{sun} + \frac{m_f \beta}{P_a} \quad (19)$$

By substituting this equation into Equation (14) and dividing by P_e , we get:

$$F = \frac{P_a}{P_e} = 1 - \frac{m_f \beta}{t_{sun} P_e} \quad (20)$$

Equation (12) provides an approximation for t_f in Case 2. Because Case 2 is a transfer performed during sunlight, Equation (12) can be used for the sunlit portion of this case, where it becomes

$$t_{sun} = 2 \left[\pi - \sin^{-1} \left(\frac{r_{\oplus}}{r(0)} \right) \right] \sqrt{\frac{r^3}{\mu}} \quad (21)$$

and can be used in Equation 20. Numerical experience shows that these approximations are close enough to obtain convergence.

In this section, we developed a set of tools that can be used to model optimal orbital transfer segments with a low level of storage. In the next section, we consider the situation where there is enough storage for the thrusters to be used throughout the eclipse.

Case Four: High Levels of Energy Storage

This case is similar to Case Three, in that energy storage is used to continue thruster operation in eclipse. The difference is that enough energy storage capacity is available to run the thrusters completely through the Earth's shadow. An example transfer segment is shown in Figure 7.

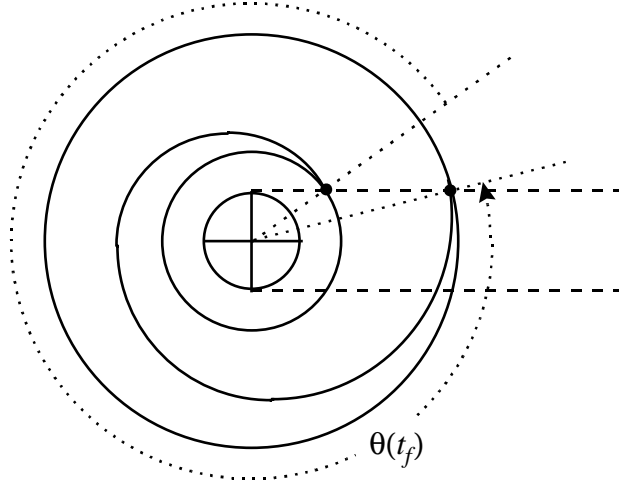


Figure 7. An Orbital Transfer Without a Coast Phase

Here, the spacecraft begins a transfer as it leaves the Earth's shadow, and completes a circle-to-circle transfer just as it is about to leave the Earth's shadow again. When many of these maneuvers are combined to create a large-scale transfer, the spacecraft will spend no time coasting between segments. Just as one segment is completed, another will begin.

The constraints for this problem are similar to those in Case Three, but the charge constraint D disappears. The charge constraint is replaced by the angle constraint:

$$\theta(t_f) = 2\pi - \sin^{-1}\left[\frac{r_{\oplus}}{r(0)}\right] + \sin^{-1}\left[\frac{r_{\oplus}}{r(t_f)}\right] \quad (22)$$

Beyond this one change, we have a problem similar to Case 3. One step in the Newton iteration is performed as:

$$\begin{bmatrix} \Delta t_f \\ \Delta \lambda_u(0) \\ \Delta \lambda_v(0) \\ \Delta F \end{bmatrix} = \begin{bmatrix} \frac{\partial \theta(t_f)}{\partial t_f} & \frac{\partial \theta(t_f)}{\partial \lambda_u(0)} & \frac{\partial \theta(t_f)}{\partial \lambda_v(0)} & \frac{\partial \theta(t_f)}{\partial F} \\ \frac{\partial u(t_f)}{\partial t_f} & \frac{\partial u(t_f)}{\partial \lambda_u(0)} & \frac{\partial u(t_f)}{\partial \lambda_v(0)} & \frac{\partial u(t_f)}{\partial F} \\ \frac{\partial v(t_f)}{\partial t_f} & \frac{\partial v(t_f)}{\partial \lambda_u(0)} & \frac{\partial v(t_f)}{\partial \lambda_v(0)} & \frac{\partial v(t_f)}{\partial F} \\ \frac{\partial G}{\partial t_f} & \frac{\partial G}{\partial \lambda_u(0)} & \frac{\partial G}{\partial \lambda_v(0)} & \frac{\partial G}{\partial F} \end{bmatrix}^{-1} \begin{bmatrix} \Delta \theta(t_f) \\ \Delta u(t_f) \\ \Delta v(t_f) \\ \Delta G \end{bmatrix} \quad (23)$$

To initialize t_f , λ_u , λ_v , and F , we use the low-thrust assumption again. Equations (10) continue to provide an adequate first approximation for λ_u and λ_v . Because the transfer is only a small perturbation to a circular orbit, the time of flight is approximately:

$$t_f = 2\pi \sqrt{\frac{r^3(0)}{\mu}} \quad (24)$$

By substituting Equations (24) and (21) into Equation (14), and solving for P_a/P_e , we get that:

$$F = \frac{P_a}{P_e} = \frac{\pi - \sin^{-1}\left(\frac{r_{\oplus}}{r(0)}\right)}{\pi} \quad (25)$$

Numerical experience shows that these approximations are adequate to obtain convergence. So, we have succeeded in creating adequate first-approximations for t_f , λ_u , λ_v , and F .

This maneuver is enabled by sufficient energy storage. If there is any doubt about whether or not the on-board battery capacity is adequate, it can be checked after the problem is solved. This is accomplished by finding the shadow-crossing time, t_{sc} , and ensuring that the following condition is met:

$$P_a(t_f - t_{sc}) \leq m_f \beta \quad (26)$$

If the condition of Equation (26) is not met, Case 4 is not the appropriate case, and Case 3 should be used to obtain a maximum radius increase for this transfer segment.

Note that this case involves a situation where it may be possible for the spacecraft to perform a complete transfer in a single segment consisting of many revolutions. Such an optimal transfer would resemble the classic outward spiral. For large transfers, extreme sensitivity to initial conditions leads to problems with convergence. This problem requires precision beyond what is readily obtained by the software and hardware used for this research. In the interest of writing robust code that can complete the required calculations in a reasonable period of time, all orbital transfers propagated in this thesis are broken into segments of approximately one orbit.

Case Five: A Final Orbital Transfer Segment Requiring Energy Storage

When a spacecraft is at the end of a large-scale orbital transfer, the scheme used to compute maximum-increase segments (Case 2, 3, or 4) either overshoots or undershoots the desired final orbit. In order to finish the transfer, a scheme designed to reach exactly the desired value of $r(t_f)$ must be used. One such scheme is used for Case One. Case One is used when the final transfer segment can be achieved before the spacecraft enters the Earth's shadow again. In the large-scale transfers propagated for this thesis, Case One is statistically the most likely scheme to be used. This is because a majority of the spacecraft's time is spent in sunlight. Occasionally, this final transfer segment requires some degree of energy storage, and a scheme resembling Case Three is used. Because the full capacity of the battery is not used, the D constraint is dropped, and replaced by an $r(t_f)$ constraint.

The Newton iteration for this case appears as:

$$\begin{bmatrix} \Delta t_f \\ \Delta \lambda_u(0) \\ \Delta \lambda_v(0) \\ \Delta F \end{bmatrix} = \begin{bmatrix} \frac{\partial r(t_f)}{\partial t_f} & \frac{\partial r(t_f)}{\partial \lambda_u(0)} & \frac{\partial r(t_f)}{\partial \lambda_v(0)} & \frac{\partial r(t_f)}{\partial F} \\ \frac{\partial u(t_f)}{\partial t_f} & \frac{\partial u(t_f)}{\partial \lambda_u(0)} & \frac{\partial u(t_f)}{\partial \lambda_v(0)} & \frac{\partial u(t_f)}{\partial F} \\ \frac{\partial v(t_f)}{\partial t_f} & \frac{\partial v(t_f)}{\partial \lambda_u(0)} & \frac{\partial v(t_f)}{\partial \lambda_v(0)} & \frac{\partial v(t_f)}{\partial F} \\ \frac{\partial G}{\partial t_f} & \frac{\partial G}{\partial \lambda_u(0)} & \frac{\partial G}{\partial \lambda_v(0)} & \frac{\partial G}{\partial F} \end{bmatrix}^{-1} \begin{bmatrix} \Delta r(t_f) \\ \Delta u(t_f) \\ \Delta v(t_f) \\ \Delta G \end{bmatrix} \quad (27)$$

Based on low-thrust assumptions, the initial approximations for λ_u and λ_v are unchanged from Equations (10). For a low-thrust transfer, the time of flight can be approximated as [6:15]:

$$t_f = \frac{\sqrt{\mu}}{a(0)} \left(\frac{1}{\sqrt{r(0)}} - \frac{1}{\sqrt{r(t_f)}} \right) \quad (28)$$

It can easily be shown that $F = t_{sun}/t_f$. By substituting Equation (21) into this relationship, we get that

$$F = \frac{2 \left[\pi - \sin^{-1} \left(\frac{r_{\oplus}}{r(0)} \right) \right] \sqrt{\frac{r(0)^3}{\mu}}}{t_f} \quad (29)$$

where t_f is already approximated by Equation (28). In the few cases that these equations are used, these approximations are found to be adequate for convergence to be reached.

Summary

In this chapter, we have developed the tools necessary to propagate optimal orbital transfer segments. Techniques for solving the boundary value problems for a number of different schemes have been developed. By piecing together a number of such segments,

large orbital transfers can be accomplished. In the chapters to follow, these tools are used to determine what advantages flywheel energy storage can yield. We also determine the conditions for which flywheel energy storage yields performance advantages.

IV. Flywheel Energy Storage Used Strictly for Propulsion

In the previous chapter, we developed a set of techniques that can be used to propagate optimal transfer segments. In this chapter, we use these as tools to examine the benefits of energy storage applied to solar electric orbital transfers. We examine the concept of adding energy storage solely for use by the solar electric propulsion system. We ignore the fact that most satellites have storage needs for their on-orbit missions, and examine the resulting mass tradeoff.

There are a number of factors that affect spacecraft performance for the transfer segments we are considering. Among these are engine type, usable flywheel battery specific energy, array specific power, overall system mass, and radius at the beginning of the transfer segment. We begin by setting most of these parameters to likely values and examining performance behavior based purely on a tradeoff between flywheel battery and array masses. Next, we examine the effects of several other factors. Finally, we simulate some large-scale orbital transfers utilizing different energy-management schemes, and compare performance figures.

Effects of a Mass Tradeoff

In this section, we examine a tradeoff between flywheel battery mass and solar array mass. Assuming that we are allocated a fixed combined mass for flywheel battery and solar array, we attempt to determine which combination maximizes the radius increase resulting from a single transfer segment. We choose a system to model, discuss how it is modeled, and discuss the information that is collected as a result.

For the system, we choose a spacecraft with an initial mass of 3000 kg. An array specific power of $\alpha = 120$ W/kg is used, which is a reasonable value for currently existing arrays [4:1235]. We assume that the usable flywheel battery specific energy is $\beta = 100$ Whr/kg, which assumes some improvement over the current state of the art [16:589], but is not unreasonable. We choose the total flywheel battery and array mass to be 150 kg. This last figure is an arbitrary selection. Different battery and array total masses will lead to different radii, because of the power that is available for propulsion. However, selection of a different value of battery and array total mass does not change the qualitative behavior that we are examining.

We model thruster capabilities based on a variant of the Xenon-Plasma Hall-effect thruster using 1.4 kW electrical power, with an efficiency of $\eta = 0.48$, and delivering a specific impulse of $I_{sp} = 1600$ seconds. In order to adjust this system's performance, we assume that thrust and mass flow rate are proportional to the power applied to it. In order for this to be a useful assumption, we need to develop thrust and mass flow rate multipliers to use. We start with the relationship[6:9]:

$$P_a = \frac{\dot{m}u_e^2}{2\eta} \quad (30)$$

where \dot{m} is the mass flow rate, u_e is the exit velocity, P_a is the electrical power applied to the engine, and η is the engine efficiency. Knowing that $u_e = I_{sp}g_0$, we can solve for the mass flow rate, and get:

$$\frac{\dot{m}}{P_a} = \frac{2\eta}{(I_{sp}g_0)^2} \quad (31)$$

Use of this equation tells us that this engine uses 3.8993×10^{-6} kg/s of propellant for every kW of power applied. Using the relationship for thrust $T = \dot{m}u_e$ and the same argument, we say that this engine provides 0.061183 N for every kW of power applied.

With this information, we examine the mass tradeoff between flywheel battery and solar array. The algorithm used is illustrated in Figure 8. The comparison begins by solving a case with a high ratio of flywheel battery to array mass. We do not start with 100% of the available mass allocated to flywheel batteries. Remember that the solar array is the only source of power, and without incoming power, no orbital transfers are possible. We increase the array to flywheel mass ratio in steps. For the first trial, we assume that there is enough energy storage available to run the engines completely through the eclipse period (Case 4). After a case is solved, the required flywheel capacity is checked. If the check proves that the current ratio provides enough energy storage to make it a valid case, the results are stored, the array to flywheel ratio is increased, and the algorithm continues to step through the first loop in the figure. If the check proves that the current case does not have enough energy storage, the second loop in the figure is enabled *before* the results are stored. This second loop is for cases that have some energy storage, but not enough to continue thruster operation throughout the eclipse (Case 3). As the array to flywheel mass ratio increases, this loop continues to run the trials and store the results. Eventually, the case of no storage (Case 2) is reached. This case is only run once, and operations cease. Cases 1 and 5 do not appear in this algorithm, because they are not designed to produce a maximum radius increase, they are designed to produce a predetermined radius increase.

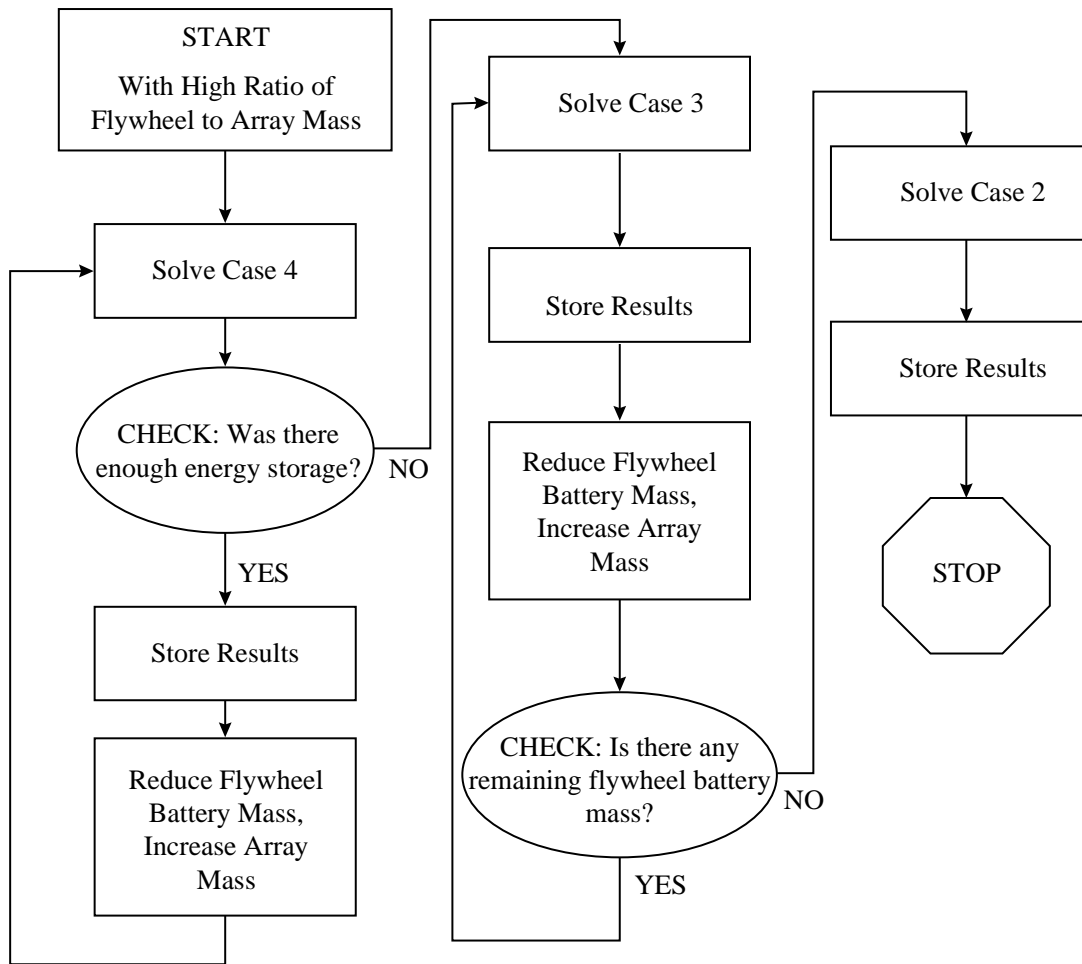


Figure 8. Algorithm Used for Comparisons Based on a Mass Ratio at a Fixed Initial Altitude.

Figure 9 shows the trajectories for each of the cases recorded, in terms of radius versus time. The key identifies the trajectories by case. Each trial creates the "S" shaped trajectory of this sort of optimal transfer. The top and bottom of each "S" are horizontal, showing that these are circle-to-circle transfers. Case 2 is the situation without storage, Case 3 is with some storage, and Case 4 is where there is enough (or more than enough) flywheel energy storage to run the thrusters continuously. Note how the final radius in-

creases as small fractions of mass are used for flywheel batteries, even though the array mass is decreasing. The final radius peaks, just before the trials transition to Case 4. After Case 4 is reached, performance drops as the flywheel battery mass exceeds its maximum useful value, and the array mass continues to decrease.

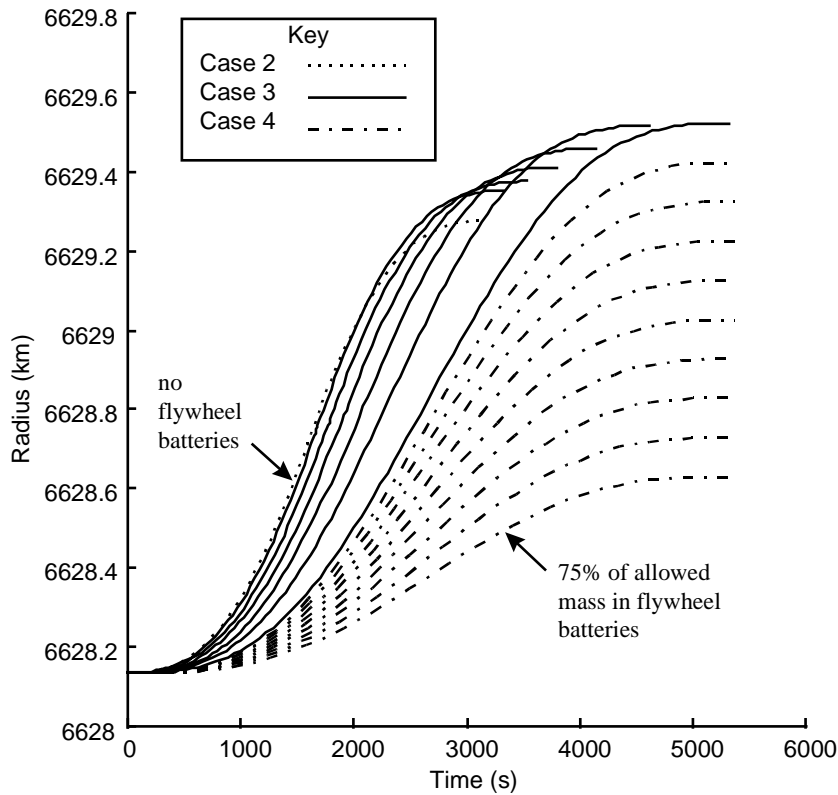


Figure 9. Trajectories For Different Flywheel to Array Mass Ratios

Figure 10 uses the same convention to label the curves, but shows the control angle histories for each case. Note that the Case 4 curves remain quite close to a zero control angle. These transfer segments are all very efficient, as they are close to the pure tangential acceleration expected of the classic slow spiral. This is the mechanism that allows energy storage to deliver more efficient transfers. Also note that the trial without

any energy storage is forced to exceed 180 degrees, creating a trace that appears to have a discontinuity.

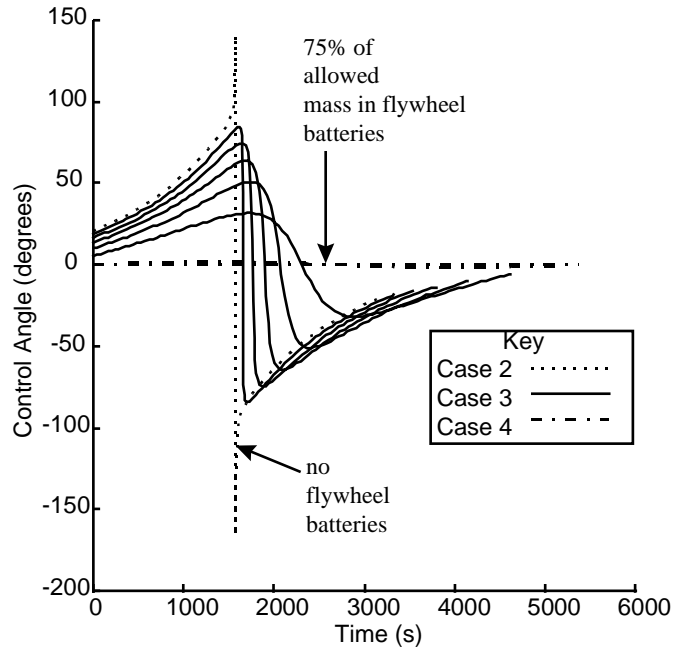


Figure 10. Control Angle Histories For Several Battery and Array Mass Ratios

From Figure 11, it can be seen that excessive mass devoted to energy storage results in small increases in radius. This is caused by the loss of mass available for the solar array, which is the only point where energy enters the system. We define the "balanced" case as the level of energy storage that is just enough for continuous thruster operation. The balanced case forms the division between Case 3 and Case 4. We reach the conclusion that energy storage beyond what is necessary to achieve this balanced case is invariably a waste of mass. This holds true, as long as we are examining single transfer segments only.

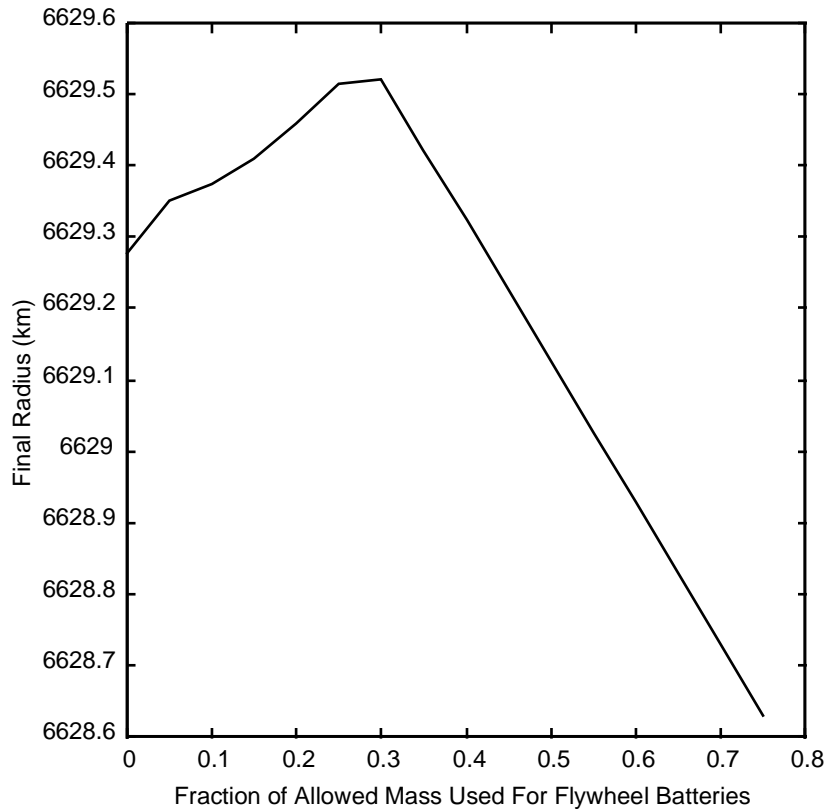


Figure 11. Final Radius Versus Fraction of Mass Allocated for Flywheel Battery

The algorithm used above spends an unnecessarily large percentage of time solving cases of no interest. These cases are the ones with more energy storage than can be used for this segment. In order to minimize wasted effort, we continue the experimentation using an algorithm that starts with the balanced case, and works towards the case with no storage. This algorithm is similar to the one shown in Figure 8, except that the loop containing Case 4 is only performed once. Rather than dictating a total mass allowed for flywheel battery and solar array masses, the solar array mass is provided for the balanced case. When the balanced case is run, the necessary battery mass is calculated. The total array and battery mass from this case is used as the total mass

allowed for the other trials. An unfortunate side-effect of this method is that trials run with different values of initial altitude will result in a different total mass. Fortunately, this does not have a significant effect on the qualitative behaviors that are exhibited, as will be demonstrated later.

We simulate a spacecraft with a 3000 kg initial mass and the same properties that we used earlier, except that we choose the array mass for the balanced case to be 100 kg. We execute the simulation for this case, and obtain the results shown in Figure 12. The radii achieved are similar to those seen in Figure 11, because the total energy storage and solar array mass are calculated to be 143 kg. Note that the best radius is reached just short of the balanced case. The balanced case is represented by "1" on the abscissa.

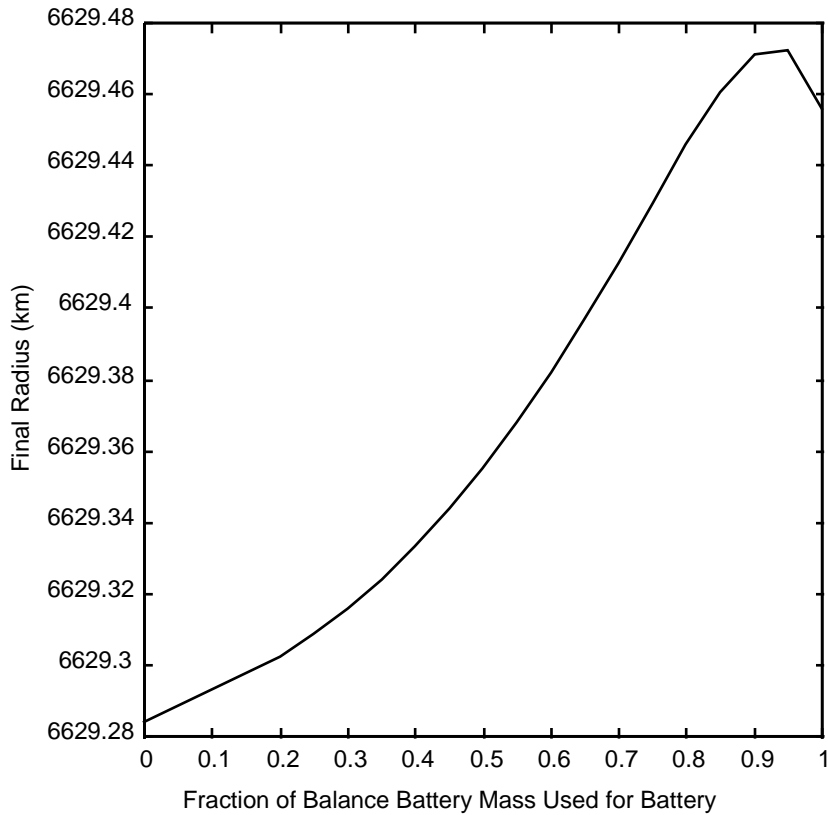


Figure 12. Final Radius vs. Fraction of Balance Battery Mass Used for Battery, in Low Earth Orbit

By running the same beginning assumptions at an altitude of 10,000 km, we get the results in Figure 13. This time, the total mass of battery and array is calculated to be 177 kg. Note that the maximum single-segment radius increase is obtained by the case with no energy storage. The initial altitude of a transfer segment plays a strong role in whether or not any benefits are realized by using energy storage. One would think that the greater time spent in eclipse at higher altitude (in the ecliptic) would favor the use of energy storage. However, the *fraction* of an orbit spent in eclipse at a higher altitude has decreased. Because of this, the transfer segment without storage achieves an efficiency

closer to what can be achieved when thrusters are used in the eclipse period. This leads to such a small efficiency improvement when energy storage is used, that the lost array mass dominates the behavior.

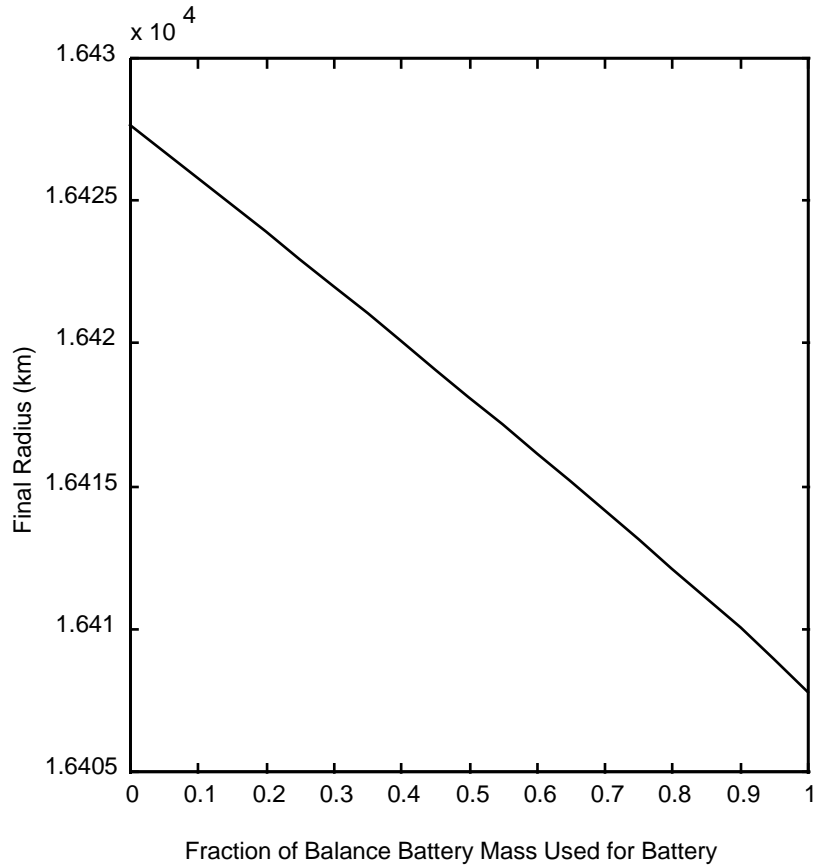


Figure 13. Final Radius Versus Fraction of Balance Battery Mass Used for Battery, for a Higher Altitude

Next, let us return to an initial altitude of 250 km. This time we use flywheel batteries with a useful energy density of only 50 Whr/kg. The results are displayed in Figure 14. Because of the lower performance of the battery system, the case with no energy storage delivers a greater increase in radius. So, we know that both altitude and battery

energy density play a part in determining whether or not energy storage is a worthwhile use of mass.

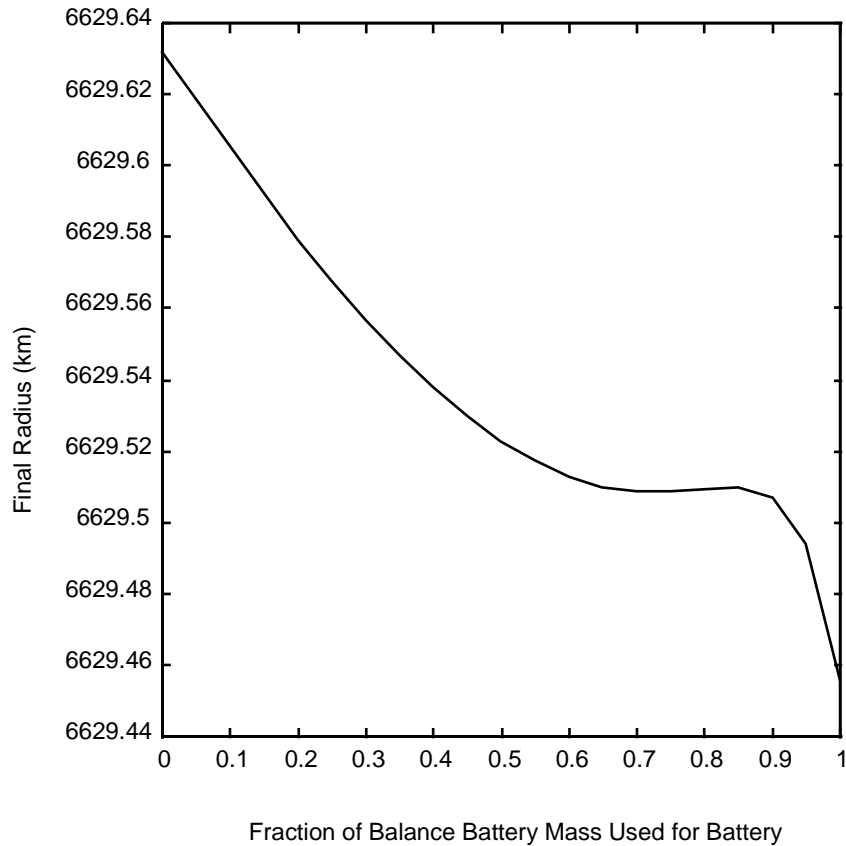


Figure 14. Final Radius Versus Fraction of Balance Battery Mass Used, for Reduced Useful Energy Density

We have established that initial altitude and usable battery specific energy are important in determining whether or not flywheel energy storage should be used for a single transfer. In the next section, we examine the effects of several other variables on when storage should be used.

Effects of Other Variables

In this section, we examine how the tradeoff between flywheel energy storage and solar array mass is affected by several additional factors. The additional factors to be examined include altitude, array specific power, flywheel battery specific energy, and engine choice. We seek to know the circumstances where flywheel energy gives an advantage.

"Break-Even" Values. Note that in Figures 11, 12, and 14 a "lump" appears between the balanced case and the case without storage. In Figure 12, it can be seen that the maximum final radius achieved is by a case that is not quite the balanced case. However, it can also be seen that the "hump" that appears is not the best combination unless the final radius values for the balance and non-storage cases are similar. In order to simplify the process of characterizing the tradeoff, we compare the final radii of the balance and non-storage cases exclusively. We seek to determine the conditions where the two values are equal, and refer to this as a "break-even" point.

Effects of Altitude and Balance Array Sizing. For the next set of trials, we find "break-even" values of usable battery specific energy versus altitude for a system with a chosen array balance mass. The algorithm used is illustrated in Figure 15. This algorithm produces a set of data points that, when plotted, compare the behavior of break-even β versus altitude for several different array and battery total masses. For each data point, an initial guess is made for the "break-even" value of β , and a secant method is used to find the actual value. This guess is made based on numerical experience, and leads to convergence in all cases.

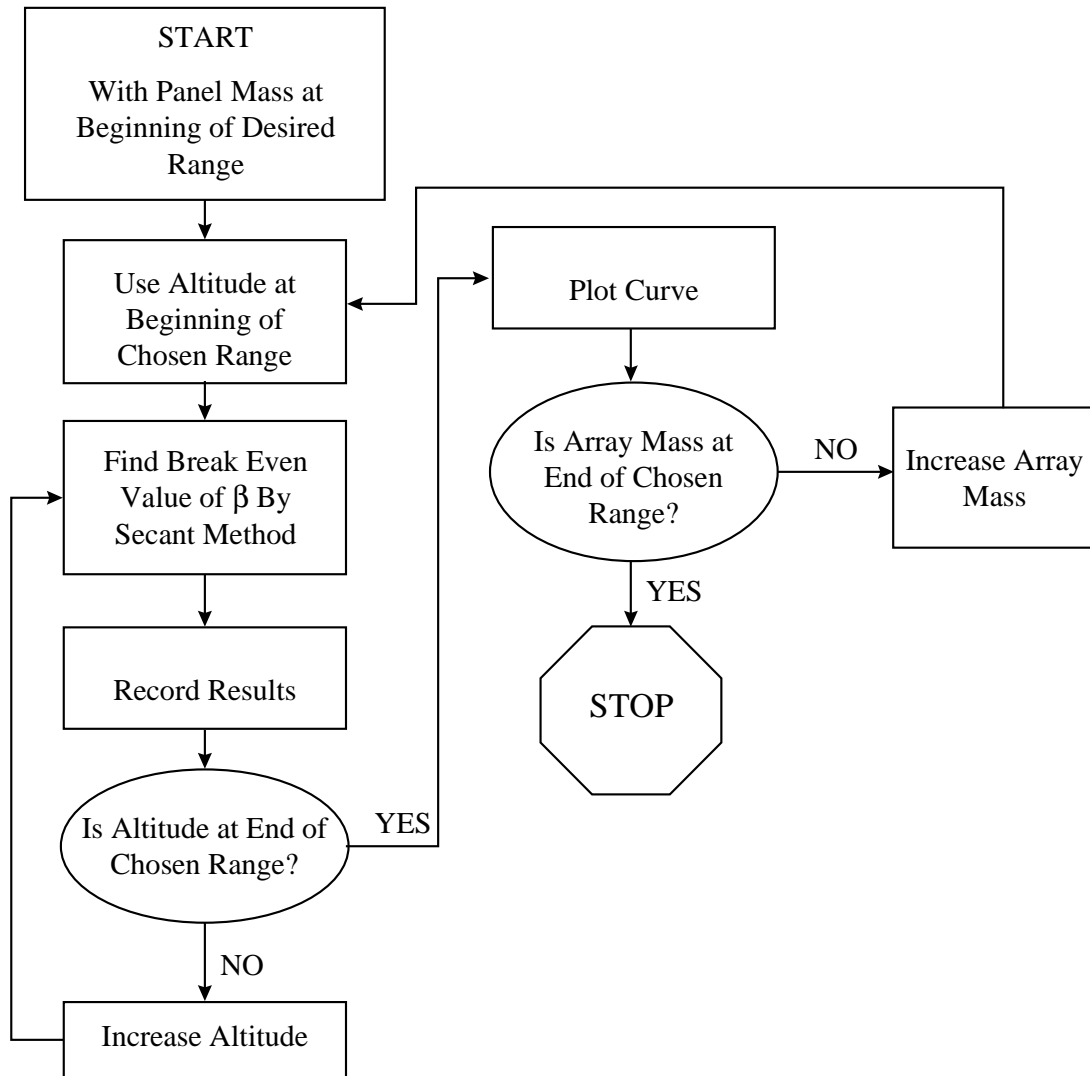


Figure 15. Algorithm For Finding Break-even Beta vs. Altitude

Here we examine the effects of altitude and the array mass chosen for the balance case. When a balance array mass is chosen, the algorithm uses that mass to calculate the balance battery mass, and the combined mass is used for the case without storage. Fixing balance array size does not fix the total array and battery mass for a range of altitudes, but we are about to show that this makes little or no difference in the behavior of the break-even values versus altitude. For these trials, we use a range of initial altitudes from

250 km to 10,000 km, an array specific power of 120 W/kg, the previously used 3000 kg spacecraft with Hall-effect thrusters, and a range of balance array masses from 100 kg to 500 kg. Figure 16 displays the results of these trials. Note that the break-even values of β are greater than 200 Whr/kg for most of the altitude range of interest. While we avoid making technology predictions that may be proven wrong, we have not seen any predictions that any operational battery systems will surpass this figure in the near future. Also, note that even when the balance-case panel mass was increased by a factor of five, the effect on the trace is not noticeable in the range of interest. Thus, we conclude that increasing system power and/or thrust does not have a significant effect on the break-even value of usable specific energy.

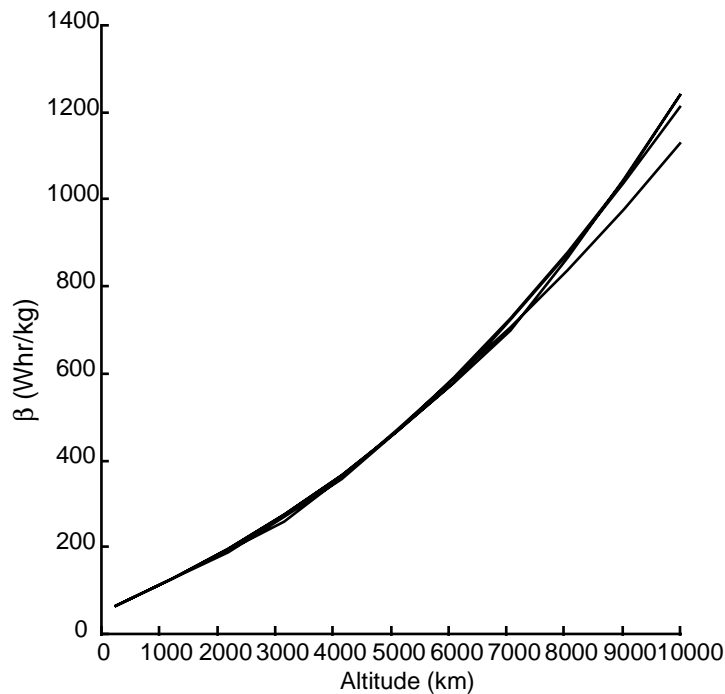


Figure 16. Break-Even Values of Beta for Different Balance-Case Panel Masses

Effects of Propulsion System Characteristics. As mentioned earlier, we assume that mass flow rate and thrust are proportional to thruster power. This limits the types of thrusters that are applicable to ones that do not use nozzles. In Table 3 we list the engines that are chosen for simulation in these trials. The first three columns of thruster characteristics, power applied (P_a), efficiency (η), and specific impulse (I_{sp}) are measured or estimated values. The last two columns show the thrust and mass flow rate multipliers as calculated using Equation (31) and the relation $T = \dot{m}u_e$. Note that we are treating the high-power systems like the others, and assume that matters of scale do not affect engine efficiency or specific impulse. These may not be the best assumptions, but they do provide a variety of system characteristics to try.

Table 3. Characteristics of Engines Simulated [21][1]

Thruster Type	P_a kW	η	I_{sp} s	Thrust Multiplier N/kW	Mass Flow Rate Multiplier kg/(kW s)
Xenon-Plasma Hall- Effect	1.4	0.48	1600	0.061183	3.8993×10^{-6}
Xenon Ion	0.5	0.55	3000	0.03739	1.2709×10^{-6}
High Power Xenon Plasma	50	0.70- 0.75	3000- 7000	0.04759	1.6175×10^{-6}
High Power Xenon Ion	5	>0.60	>2500	>0.05	$>2.0 \times 10^{-6}$
Pulsed Magnetoplasmadynamic	12	0.75	6116	0.02500	4.1698×10^{-7}

Now we examine the effect of propulsion system characteristics on the break-even values of usable energy density for a range of altitudes. The algorithm used is similar to that shown in Figure 15, but instead of varying the balance array size we vary the thrust and mass flow rate multipliers. Using the five thrusters listed in Table 3, we get the plot

shown in Figure 17. In the range where the break-even values of β are reasonable, the thruster characteristics make no significant difference.

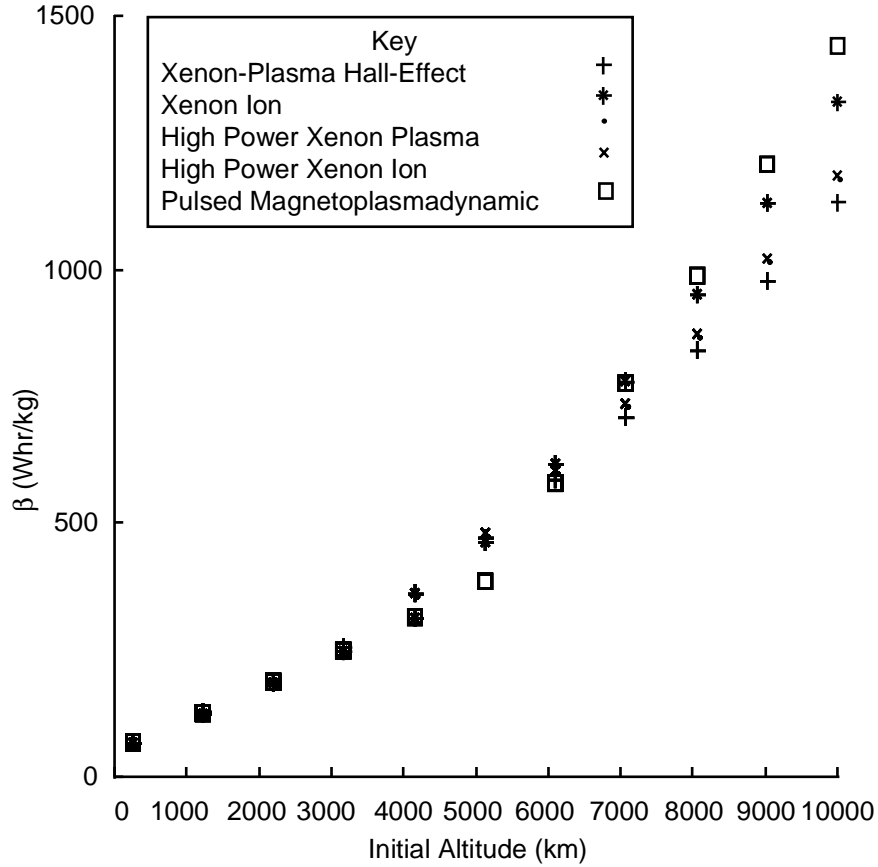


Figure 17. Break-Even Values of Beta for Several Different Sets of Engine Characteristics

Effects of Array Specific Power. Because we have been examining a mass tradeoff to find the best combination of flywheel batteries and solar array, it is only natural to think that the array specific power (α) would have an effect on the break-even value of usable energy density (β). Now we examine this relationship. We use a 3000 kg spacecraft with a Hall-effect thruster and 100 kg of array mass for the balance case. We

examine the break-even value of β for a range of α from 50 to 200 W/kg. Repeating this for several altitudes, this algorithm delivers the results shown in Figure 18.

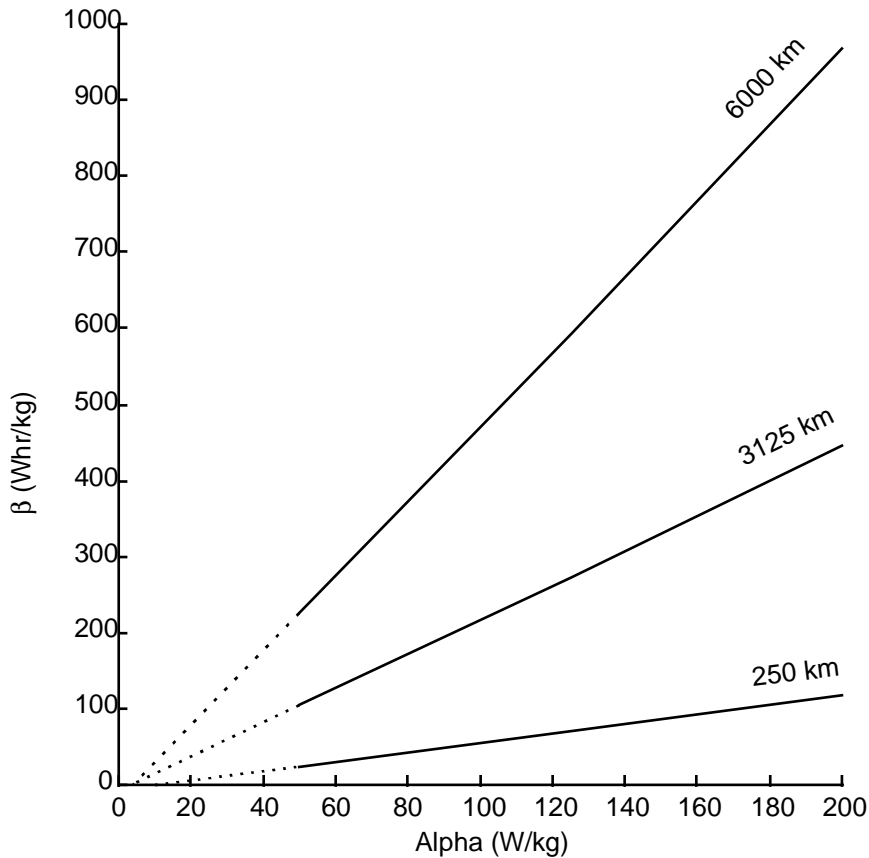


Figure 18. Break-Even Beta Versus Alpha For Several Altitudes

Dotted lines have been added to this plot to show that the traces can be extrapolated to pass close to the origin. Therefore, these lines represent a nearly linear relationship where break-even values of β vary directly as α . Seeing that these ratios make a strong contribution to determining the effectiveness of energy storage, it is natural that we should seek an equation to estimate the slope of these lines. Figure 19 shows the scatterplot that results from using several combinations of array masses and engine types and

finding the break-even values of β/α for different altitudes. Even though we have shown that mass and engine choices are not strong contributors to the effectiveness of energy storage use, their combined effects can be considerable. This leads to the conclusion that there is not a valid, simple relationship that relates break-even values of β/α to altitude.

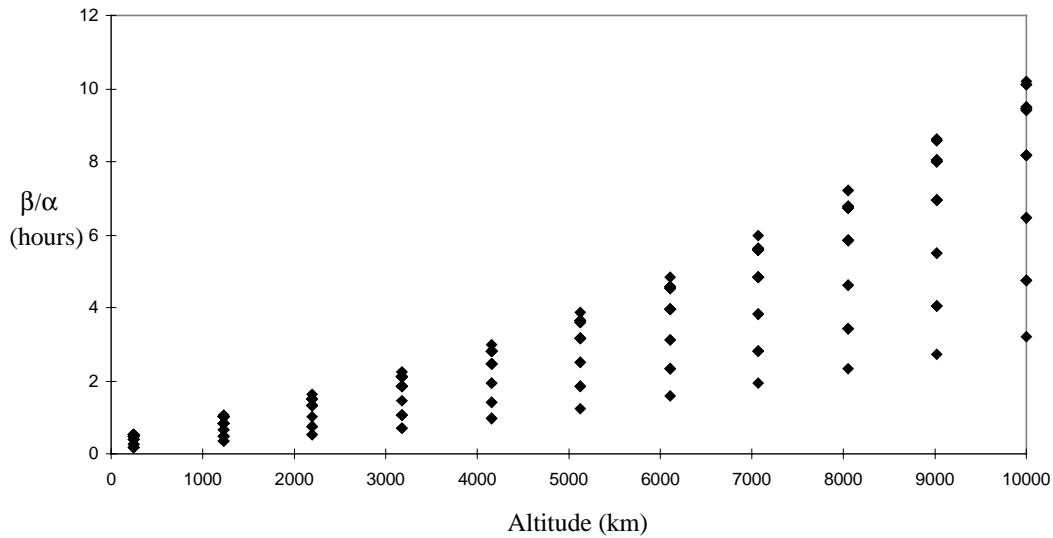


Figure 19. β/α for Many Configurations and Altitudes

In this section, we examined the tradeoff between array and battery mass, and developed some "feel" for how flywheel energy can pay off in a larger radius increase for a single transfer segment. We have also examined how other factors affect the utility of energy storage, including altitude, engine type, and the masses of the power and energy storage systems. The practical use for these relationships is to assist in designing systems to accomplish large orbital transfers. In the next section, we examine the effect of flywheel energy storage on a spacecraft making such a transfer.

Concepts Applied to a LEO to GEO Transfer

Examination of transfers on a segment-by-segment basis is instructive, but a practical orbital transfer would require tens to thousands of transfer segments. In order to find out what effect flywheel energy storage has on a large orbital transfer, we need to run simulations involving many transfer segments. Not only does this allow us to see what time-savings energy storage may provide, but it allows us to examine how efficiently propellant is used. Final masses calculated in a segment-by-segment analysis are not very informative, as configurations that provide smaller radius increases tend to use less propellant. This does not tell us much about how *efficiently* propellant mass is used. When we compare transfers that have an actual goal for a final radius, we obtain practical knowledge about this issue.

Because the break-even value of usable energy density (β) increases rapidly with altitude (see Figure 17), we do not expect to see a faster LEO to GEO transfer resulting from the use of energy storage. However, because of the comparatively long period of time spent at low altitudes in a low-thrust transfer, we could find that it results in a shortened transfer time. We must run a simulation to find out.

A flowchart of the algorithm used to propagate large orbital transfers is displayed in Figure 20. For each transfer segment, the initial values are converted to canonical units. Then, the appropriate routine is called to solve the boundary value problem. If there is some question about which case should be solved, Figure 21 illustrates the process used to select the best one.

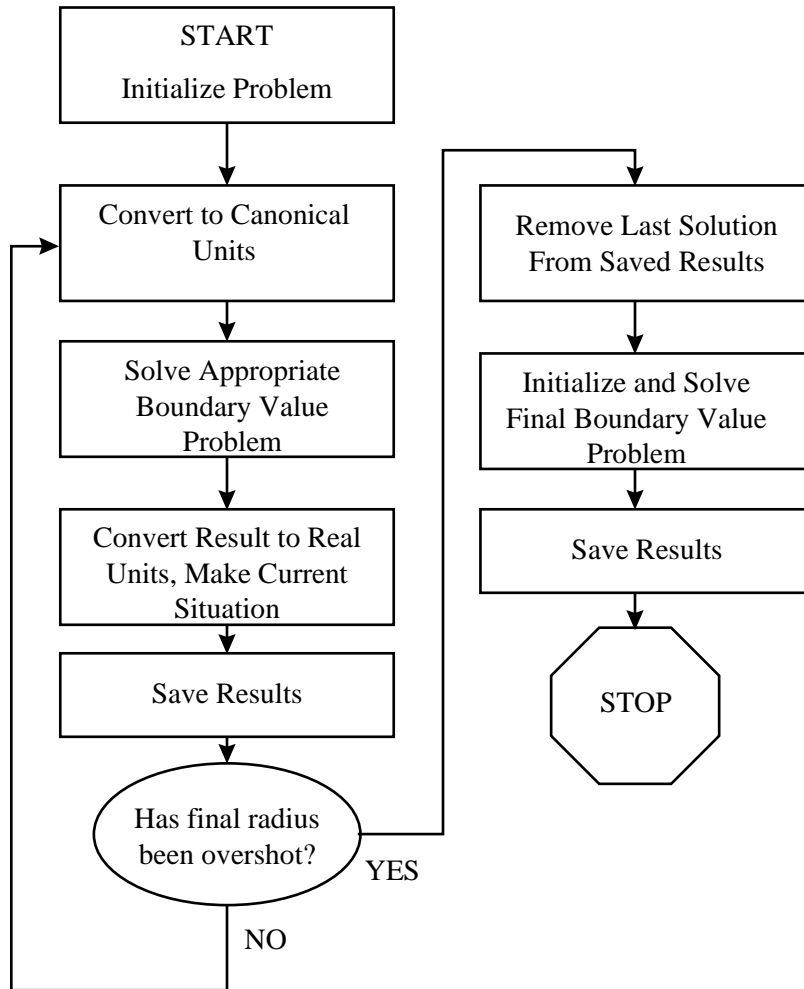


Figure 20. An Algorithm for Simulating a Large Orbital Transfer

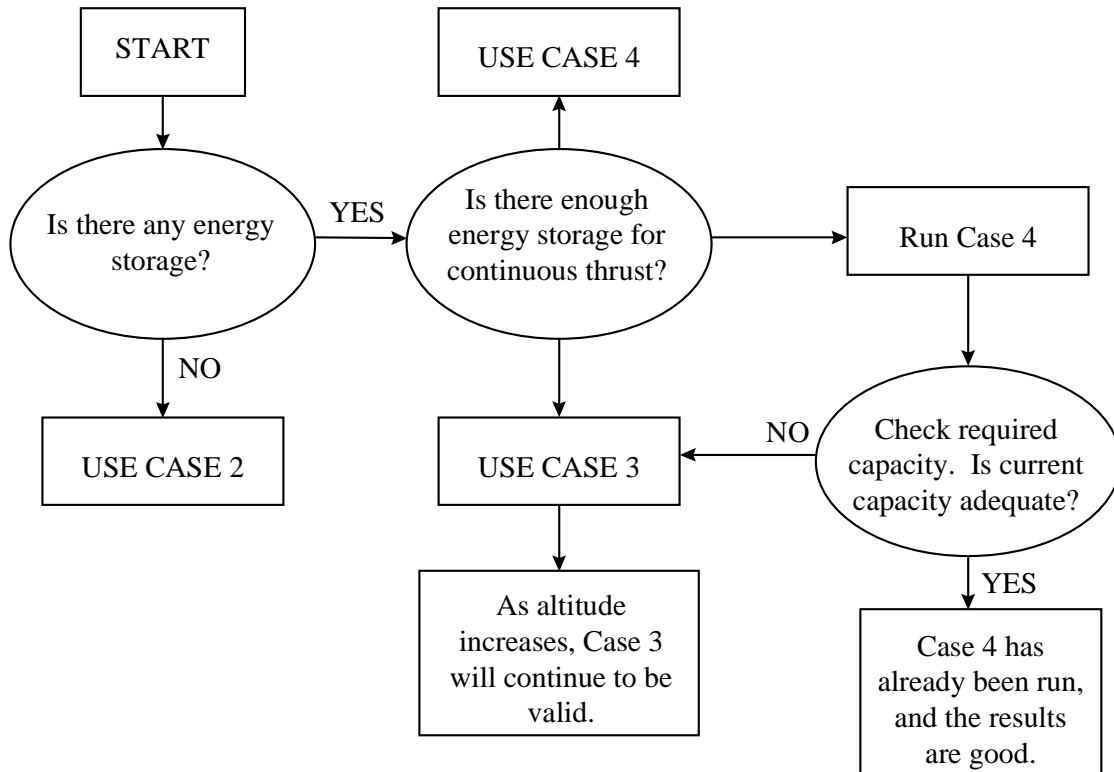


Figure 21. Algorithm for Determining Appropriate Case

The problem is initialized as a 3000 kg spacecraft in a circular parking orbit with a 250 km altitude. We choose to use the Hall-effect thruster, a usable battery energy density of 100 Whr/kg, and an array specific power of 120 W/kg. Two transfers are propagated, one without storage and one with a degree of storage optimized for the highest performance at low altitude from examination of Figure 12. Both systems have a total array and battery mass of 717 kg. For the transfer without storage, the array is 717 kg. For the case with storage, the array mass is 522 kg and the battery mass is 195 kg.

Figure 22 illustrates radius with respect to time for the two systems being compared. First of all, it should be noted that both systems overshoot their target, geosynchronous orbit, because the portion of the algorithm designed to use Case 1 or Case 5 to

get the right final radius is not implemented. Toward the end of these transfers, the increases made by individual transfer segments are several thousand kilometers apiece. Though the end of the transfers is not tidy, the trends are clear. The spacecraft that does not use any storage wins a race to geosynchronous orbit. Figure 23 is a magnified view of the radius versus time results for the first 15 days. Note that the spacecraft with storage is winning the race until some point after a radius of 8000 km. The time spent getting to the final orbit is not the only matter of interest, though. We are also interested in which system makes the most efficient use of propellant mass.

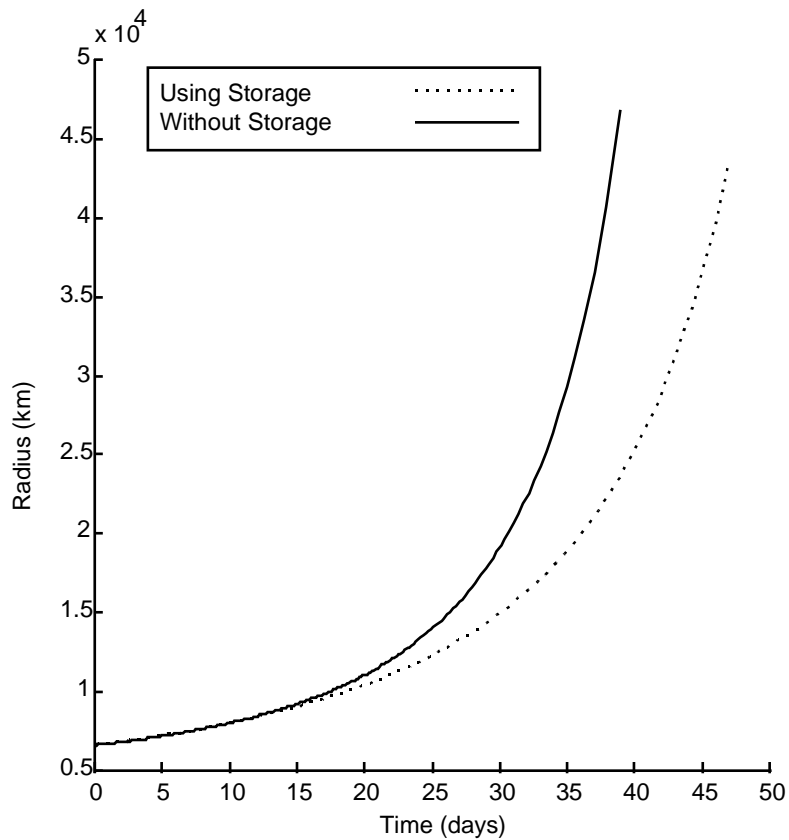


Figure 22. Radius Versus Time, For Two Spacecraft Configurations

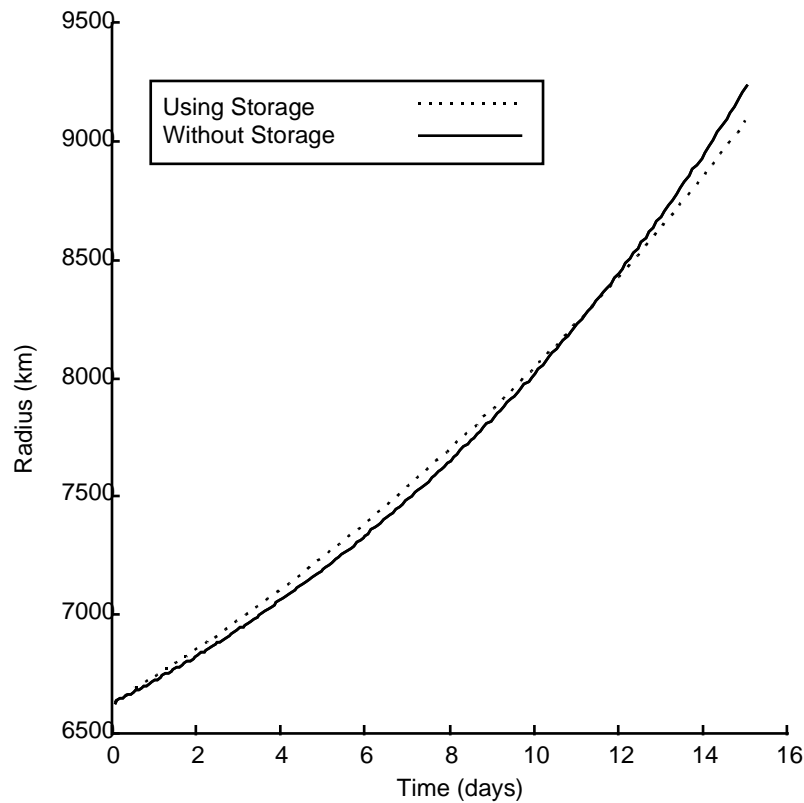


Figure 23. Radius Versus Time For the First 15 Days

Figure 24 shows the results when we plot remaining spacecraft mass against achieved radius. The system that used energy storage lost a race in terms of time, but realizes a great benefit with respect to the mass of the payload that can be delivered to any altitude. The payload mass delivered to GEO by the system using energy storage is approximately 100 kg larger, though it takes about 10 days longer to get there. Remember that the flywheel battery mass does not encroach on the payload mass, because the total battery and array mass is equal to the array mass for the case without storage. Several similar comparisons have been run, and this trend is consistently observed.

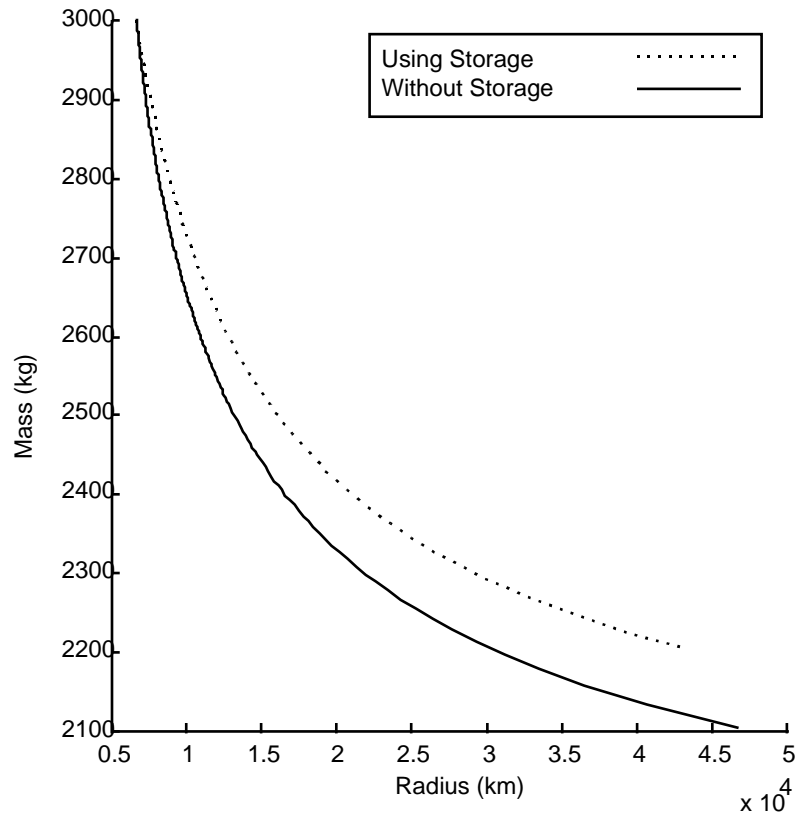


Figure 24. Spacecraft Mass Remaining With Respect to Radius Achieved

In this section, we compared a system using no storage to a system of equal mass, with some of its array mass replaced with a flywheel battery system. The results show that the system with flywheel storage takes longer to reach a geosynchronous orbit, but does so more efficiently. This is because systems that use energy storage are capable of performing transfer segments with a minimum of control angle adjustment, as seen in Figure 10. Because control angles are kept to a minimum, the spacecraft does not waste excessive propellant recircularizing the orbit at the end of each segment.

Conclusions

In this chapter, we have examined the use of energy storage expressly for the use of the propulsion system. We examined many of the characteristics of orbital transfer segments. We have found that systems that use such storage can decrease the time spent in performing transfers near the Earth, but are not likely to do so in reaching high Earth orbits. Though spacecraft using energy storage take longer to reach higher Earth orbits, they allow a spacecraft to do so with a higher propellant efficiency. These higher propellant efficiencies can be used either to decrease the mass of the spacecraft that has to be put into low Earth orbit, or to increase the payload mass that can be delivered. In the next chapter, we examine slightly more realistic cases, where spacecraft have minimum power and storage requirements. This furthers the understanding how flywheel energy storage can be used advantageously.

V. Flywheel Energy Storage Baselined for On-Orbit Needs

In this chapter, we recognize that satellites have missions to perform after they are moved to a higher Earth orbit. In the previous chapter, we examined a tradeoff between array and battery mass based on the concept that no minimum energy storage capacity is required. Because all likely missions have power requirements and must continue to operate when in eclipse, they have energy storage and power requirements. In this chapter, we examine orbital transfers for a satellite with large power and energy storage requirements using no additional array or battery mass. Then, we examine this same spacecraft with additional mass allotted for array and battery, and determine the best combination to use.

Spacecraft With Minimum Requirements

In this section, we begin with a spacecraft with some high power requirements for its on-orbit mission in a geosynchronous orbit. Because this spacecraft must not cease operation when it passes through the Earth's shadow, it has a requirement for energy storage. We assume that all of the power provided by the solar array can be used for propulsion during the spacecraft's LEO to GEO transfer, and that we are not allowed to carry any additional mass for a larger array or battery to use for this transfer. There are two extreme approaches that can be used to perform this transfer. The spacecraft can rely on its panels alone and perform a discontinuous transfer, or it can make use its battery storage capacity and perform a transfer without any coast periods.

The spacecraft is chosen as one with a parking-orbit mass of 3000 kg, and has a payload power requirement of 10 kW. During the period when a satellite at this altitude would have maximum eclipse, we know that the following power balance must be met:

$$P_e t_{sun} = P_L t_{orb} \quad (33)$$

Here P_e is the power available from the solar array, t_{sun} is the period of sunlight in one orbit, P_L is the payload's power requirement, and t_{orb} is the period of one orbit. In order to meet the worst-case eclipse conditions, the panels must be capable of collecting some excess power that can be saved for use in the Earth's shadow. Solving this equation for P_e , the 10 kW payload requirement results in a need to collect approximately 10.5 kW. If the arrays have a specific power of 120 W/kg, they have a mass of 87.5 kg. The capacity of the battery system must be:

$$m_f \beta = P_L t_{sh} \quad (34)$$

where m_f is the battery mass, β is the usable energy density, and t_{sh} is the maximum period spent in eclipse. Using this relationship, and the value $\beta = 100$ Whr/kg, we find that the minimum battery mass is 116 kg.

The algorithm used for these transfers is the same as the one illustrated in Figure 20. The difference lies in the choice of the appropriate boundary value problem to solve. We are comparing a transfer where the flywheel batteries are utilized to one where they are not. For the first trial an orbital transfer based on the Case 2 boundary value problem is propagated, where no energy storage is used. For the other transfer, Case 4 is used. Because the energy storage available is designed for an eclipse situation found at geosynchronous, the last maximum increase segment is the only one that is likely to come close

to using the entire capacity of the battery system. Because of some uncertainty in this area, the algorithm shown in Figure 21 is used to ensure use of the appropriate case.

Transfers are simulated for the described system using both schemes. The results are shown in Figures 25 through 27. These figures describe the transfer making use of energy storage as "continuous," because this scheme is able to perform transfers without coast periods. The other scheme is labeled "discontinuous," as all transfer segments are performed in sunlight only. Figure 25 compares the radius versus time profiles for both trials. The system not using the available energy storage is at a clear disadvantage, as it takes 40 days longer for it to reach geosynchronous radius.

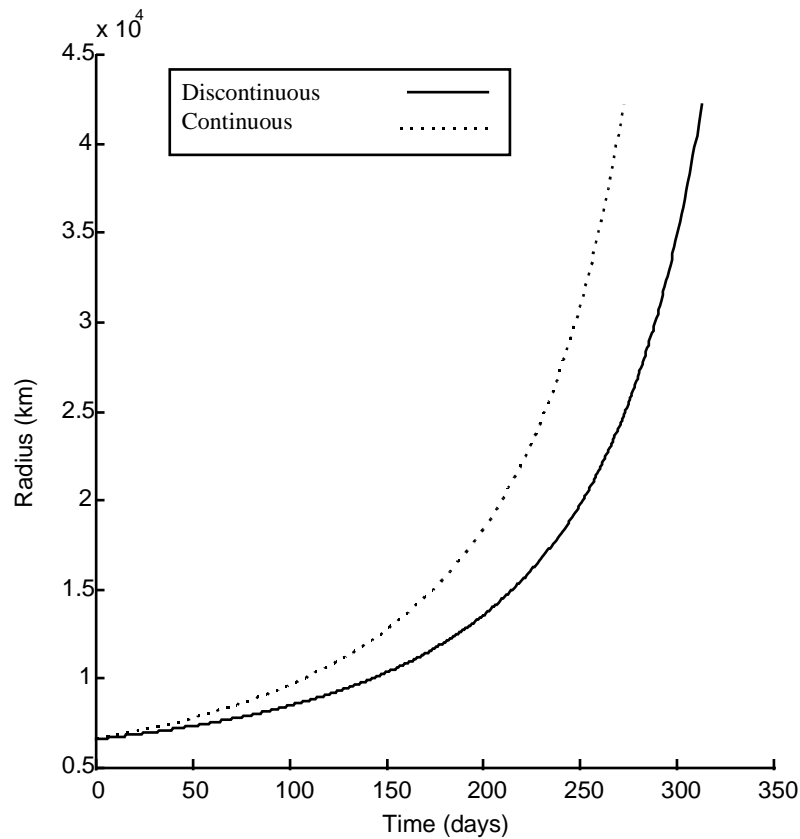


Figure 25. Radius Versus Time Comparison For Two Transfer Schemes

Figure 26 shows single segment radius ratios with respect to each segment's beginning radius. This information is analogous to a rate of increase. Notable in this plot are the discontinuities found at the end of the traces. These are caused by the final transfers, whose goal is not to maximize radius, but to achieve exactly the desired radius. Note that the lines cross at a radius of approximately 20,000 km. For lower radii, the scheme using energy storage provides the largest increase per transfer segment. For radii above this, the scheme not using energy storage provides better results. If we are interested in merely minimizing the transit time, it is a good idea to quit using the flywheel batteries at this point.

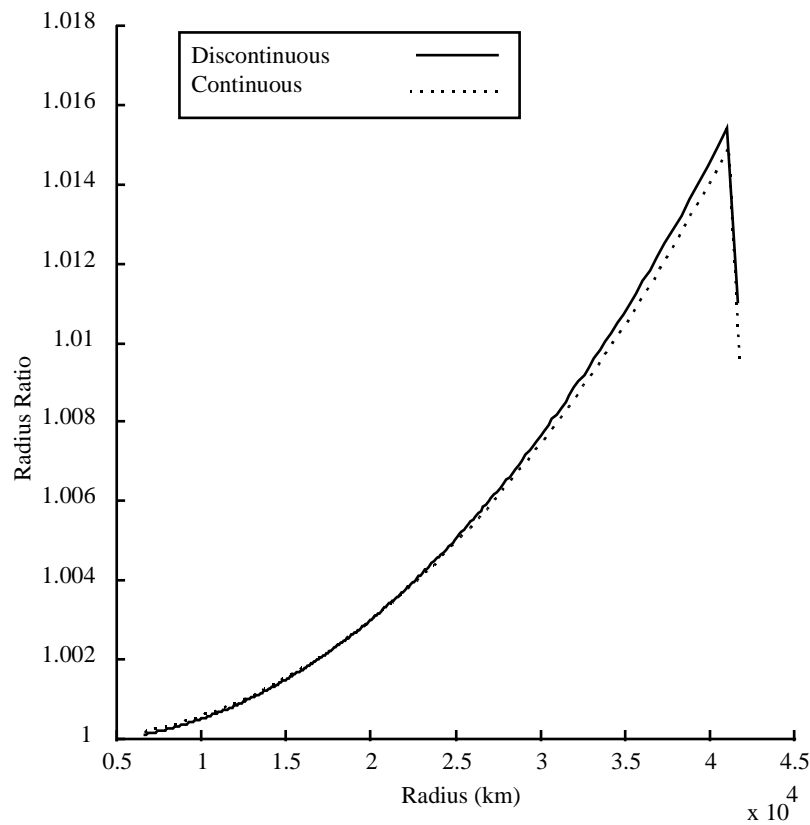


Figure 26. Radius Increase Ratios Versus Radius Comparison

Figure 27 compares the propellant use of the two trials. The scheme using energy storage has a clear advantage: Approximately 98 kg of propellant are saved by making use of the spacecraft's energy storage.

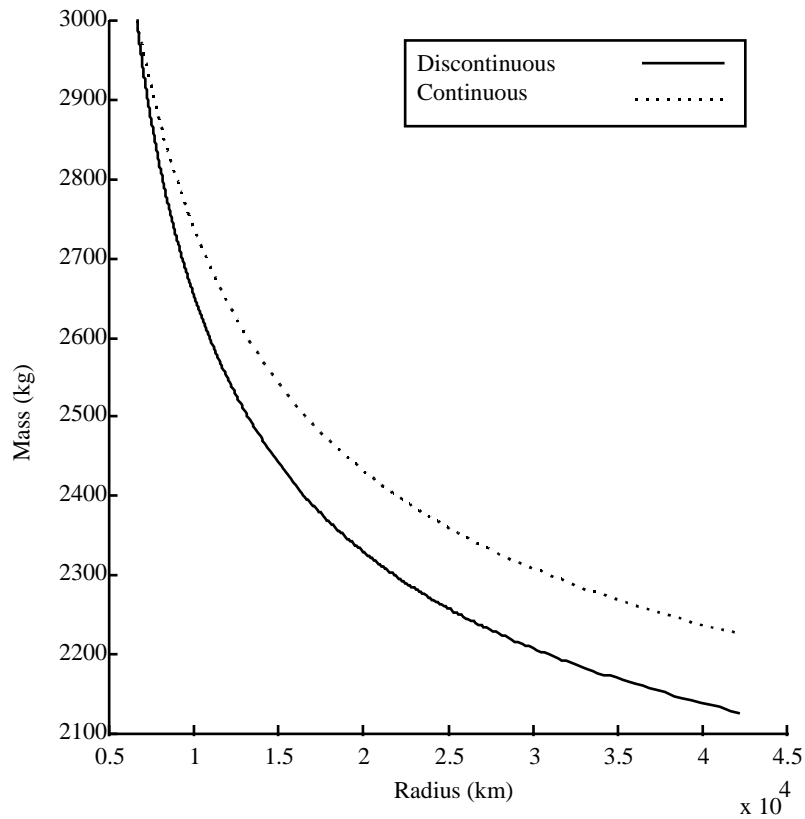


Figure 27. Mass Versus Radius Comparison

Adding Additional Battery and Array Mass

After examining a spacecraft's orbital transfer performance with only its minimum power and energy storage requirements, it is natural to ask how additional mass allocated for the use of power and energy storage would be best used. In this section we use the spacecraft characteristics from the previous section, but assume that we have an

additional 100 kg of system mass that can be used for solar array and battery mass. We determine how much of that mass should be used for increasing the size of the solar array, and how much of that mass should be used to increase flywheel battery capacity.

The spacecraft in the previous section required 87.5 kg of array mass and 115 kg of battery mass. The spacecraft's initial mass remains at 3000 kg, but we use another 100 kg of this mass for array and battery. First, we look at two extreme cases. One extreme is where we use all of the additional mass for array. Having 100 kg more array provides the spacecraft with more power, and higher thrust. With this configuration there is not enough battery storage for continuous thrust through the eclipse as higher altitudes are reached. The percentage of time spent in eclipse is low when this occurs, and it might not have a negative impact. The other extreme is a "pseudo-balanced" configuration. As was shown in the previous chapter, battery capacity that is not used is wasted mass. The second to last transfer segment requires the most energy storage, if it is to be a transfer with no coast period. Remember that the last transfer segment is typically a correction, that we assume to be small for this approximation. We make a low-thrust assumption, approximating the last transfer segment as a circular orbit at GEO. Using Equations (33) and (34), we find that 56.75 kg of the additional mass should be used for flywheel battery mass, and the remaining additional mass should be used for the solar array.

These two spacecraft configurations are used in a simulated fly-off. The results are illustrated in Figure 28 and Figure 29. Figure 28 illustrates orbital radius versus time for both configurations. The solid curve represents the configuration where all additional mass is used for increased array size, which is labeled "array only." The dotted curve is for the "pseudo-balanced" configuration. The configuration where only array mass is

added clearly has an advantage in minimizing transit time, as it arrives at a geosynchronous radius 54 days before the other configuration does. This configuration takes 946 transfer segments and 128 days, while the "pseudo-balanced" configuration takes 1355 segments and 182 days. Figure 29 shows the mass versus radius curves for the two configurations. The "pseudo-balanced" configuration saves approximately 12 kg of mass, but the mass used by both configurations is so similar that Figure 29 appears to have only one trace.

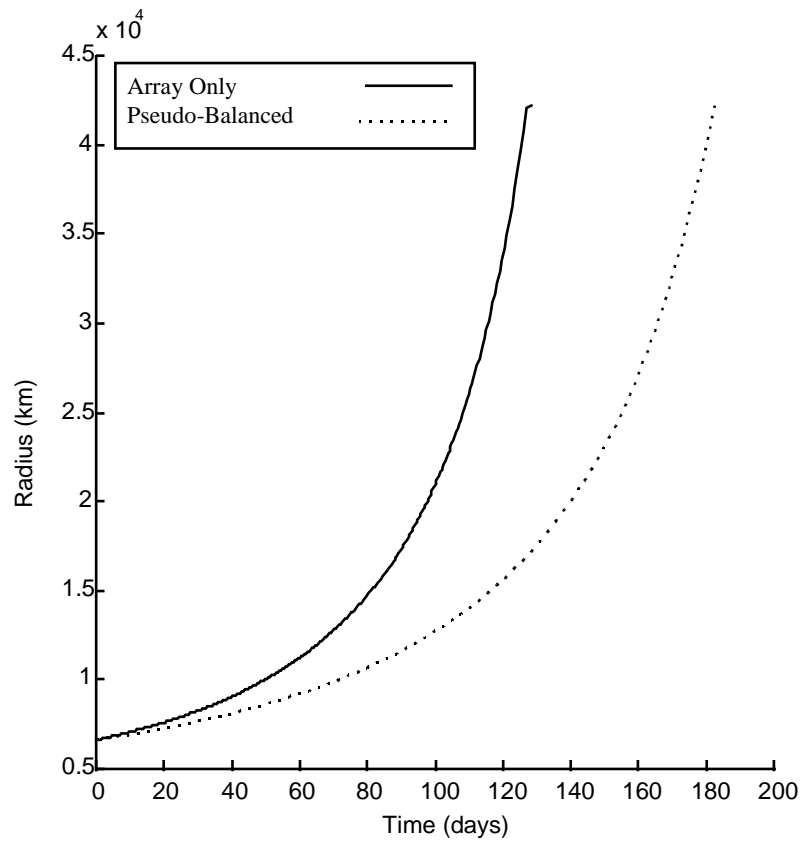


Figure 28. Radius Versus Time for Two Extreme Configurations

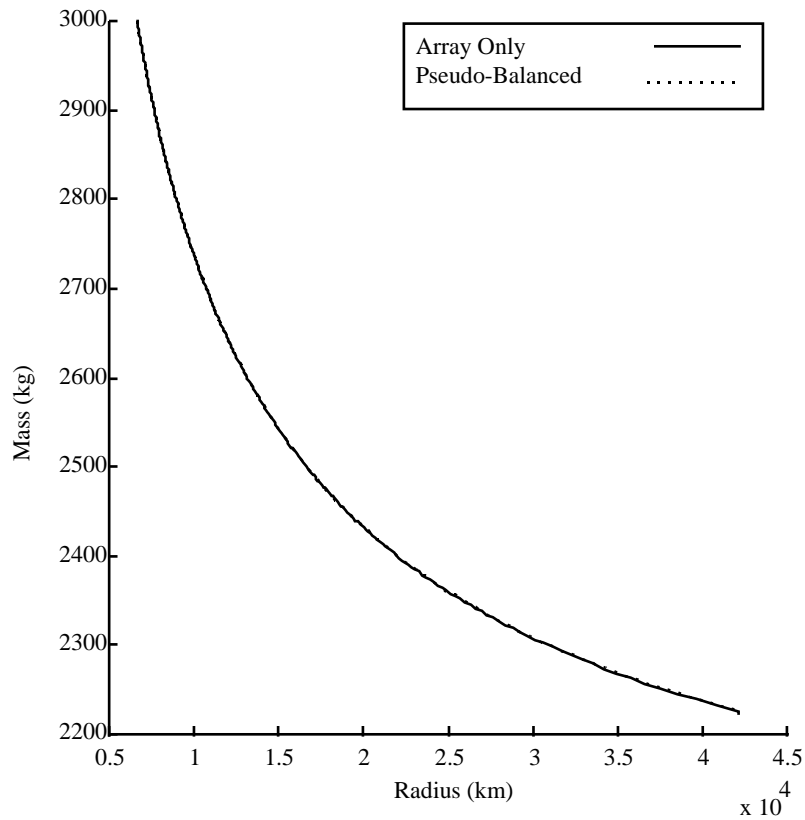


Figure 29. Mass Remaining Versus Radius for Two Extreme Cases

The preceding results do not give a complete picture, because we do not have any indication of the behavior that will be exhibited between these two extreme cases. It is necessary to consider other cases to determine what is the best configuration. The system is simulated again, and four intermediate cases are added. The results are shown in Figures 30 through 33. Nothing remarkable is displayed, the behavior between the two extremes is quite predictable. Values for the intermediate configurations fall between the values for the two extreme cases in all of these plots.

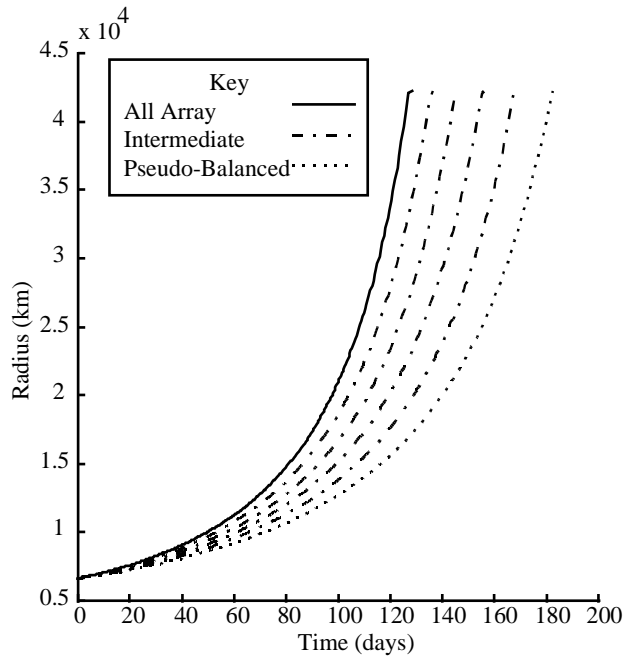


Figure 30. Radius Versus Time With Intermediate Cases Added

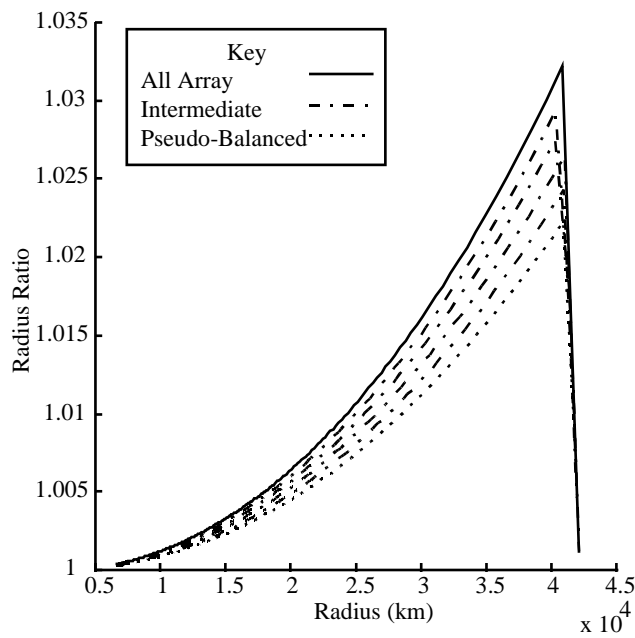


Figure 31. Radius Ratio Versus Initial Radius With Intermediate Cases

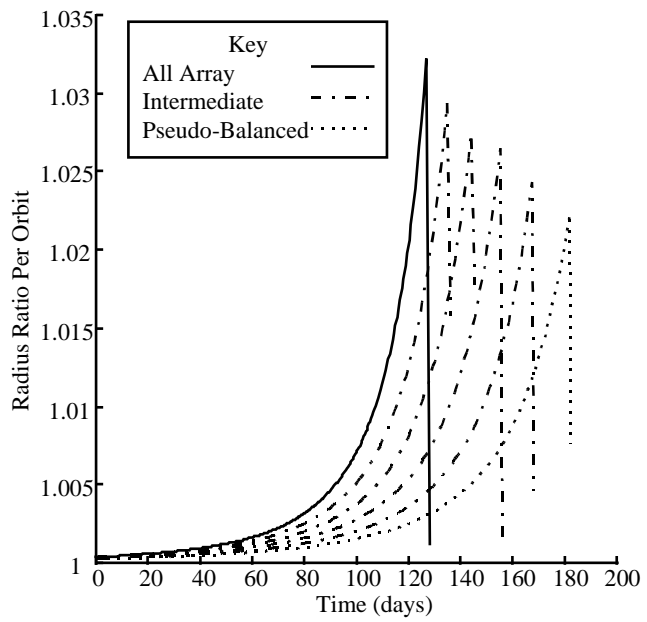


Figure 32. Radius Ratio Versus Time With Intermediate Cases

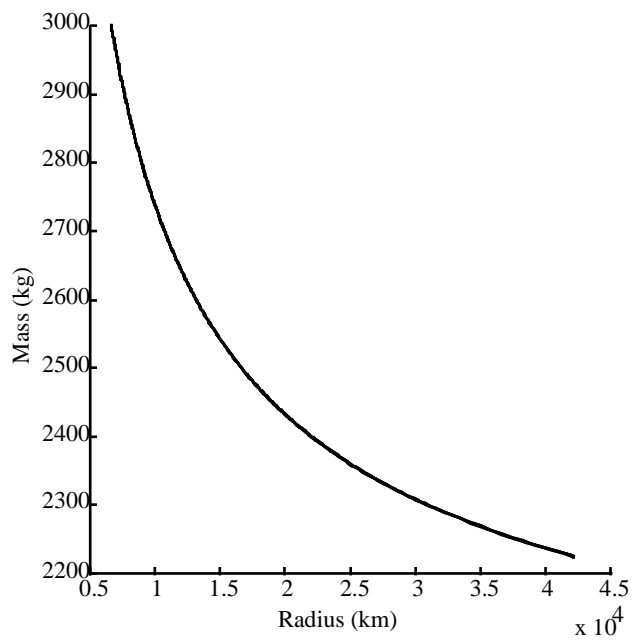


Figure 33. Mass Versus Radius With Intermediate Cases

From examination of this tradeoff, we determine that in this case the baseline level of energy storage is adequate for use in the transfer from low Earth orbit to geosynchronous orbit. Additional mass allocated to flywheel energy storage can save a bit of mass, but the transit time is greatly increased. Here, we have reached a point where additional battery mass delivers diminishing returns.

Summary

In this chapter, we examined a system with some on-orbit requirements for energy storage and power. Simulations are run where the spacecraft completes a large-scale orbital transfer with no additional energy storage or power. A comparison is made between two schemes, one where the available energy storage is not used, and one where the energy storage is used to the full extent possible. The second scheme resulted in a transfer without any coast periods, delivering a significantly increased payload mass in a shorter period of time.

Next, we examined the same system, but with an increased mass allocated for flywheel batteries and solar array. Keeping the system's minimum energy storage and power requirements in mind, we studied a tradeoff between additional array and battery mass. It is found that using much of the additional mass for flywheel batteries results in a much longer transit time, though a small amount of propellant is saved. The configuration where all of the additional mass was devoted to array provides a greatly improved transfer time, though it uses slightly more propellant mass.

VI. Summary, Conclusions, and Recommendations

Summary

Several different orbital transfer scenarios have been presented, each with its own set of boundary conditions. Schemes for obtaining optimal, constant-thrust transfer segments have been developed for each scenario. These transfer segments have been used individually to evaluate tradeoffs between solar array and flywheel battery mass under a variety of different conditions. Transfer segments have been linked together to form large-scale transfers. An example large-scale orbital transfer was used to examine the battery and array tradeoff further. A more realistic situation was introduced, where a spacecraft's payload creates minimum requirements for energy storage and power. This spacecraft performed a pair of simulated large-scale transfers using a configuration that provided it with only the minimum necessary energy storage and power. When this spacecraft's design allowed it to use a larger mass for propulsion, a new mass tradeoff was examined.

Conclusions

This work examined how flywheel energy storage can be used to improve the efficiencies and transit times of orbital transfers utilizing solar electric propulsion systems. Some related work has been accomplished on this concept, but the full benefits that are available cannot be realized without the use of optimal orbital transfers.

When single transfer segments were examined, we found that the use of flywheel energy storage can lead to larger transfers. This is true when usable energy density is

high, and the transfers begin in LEO. As initial altitude is increased, this advantage fades. Higher usable energy densities can counter this effect, but the energy density levels required quickly become unreasonable. The qualitative nature of this problem is not strongly affected by thruster choice, or array and battery total mass.

When a spacecraft has flywheel energy storage solely for the use of the solar electric propulsion system, we found that trading solar array mass for energy storage mass led to an increase in transit time for large transfers. This increase in transit time may be outweighed, however, by the propellant mass saved. The example solved in this text shows a case where the utilization of energy storage leads to a 10 day increase in transit time, but saves approximately 100 kg of propellant. For most mission-planning scenarios, this would be a welcome trade.

When a spacecraft's on-orbit needs are taken into consideration, and these resources are available to the solar electric propulsion system, the use of flywheel energy storage becomes even more useful. By using the energy storage that already has to be on board, savings in both transit time and propellant mass can be realized. When a spacecraft's design allows for additional mass to be added in the form of array and battery masses, the tradeoff will have to be considered carefully. Because the example in this text was for a system with large baselined power and energy requirements, increasing battery mass provided diminishing returns, while significantly increasing transit time. Under these conditions, the designer may decide to put all of this additional mass into the solar arrays. When systems with lower baselined power and energy needs are put into the same situation, the results will possibly be different.

Recommendations

It is the nature of research that when any question is answered, several more questions are proposed. It is only natural that there are more questions to ask, and that improvements can be made to the models used in this work. Many assumptions are made to simplify the problems approached. By reducing the number of parameters that are considered, these problems become more manageable. Assumptions were made about the Earth's shadow, solar array efficiency, power system efficiencies, and a number of other subjects. In this section, we seek to provide suggestions to improve these assumptions for anyone who would choose to explore this subject further.

The shadow model is simplified by keeping the problem in the ecliptic plane. This places the spacecraft in a worst-case scenario when solar electric propulsion is used. As the percentage of time spent in eclipse per orbit increases, the advantages gained by using energy storage increase. Remaining in the ecliptic provides a best-case scenario when one wishes to prove the effectiveness of an energy storage scheme. Trajectories that leave the ecliptic are purposely avoided in order to reduce the degrees of freedom that have to be examined. For example, we could have decided to perform large-scale transfers in the Earth's equatorial plane. This is a more likely scenario for a spacecraft that is enroute to a geostationary orbit. For fair comparisons between spacecraft configurations to be made, each large-scale transfer would have to be optimized with respect to the time of the year that it began its transfer. This optimization would have significantly increased the complexity of and computation time for these problems. Allowing for three-dimensional trajectories would have had a similar effect.

Another assumption made is that solar array efficiency is constant with respect to time. When long periods of time are spent at medium earth orbit altitudes, this is not true. The radiation present causes significant solar array degradation. Incorporating these effects would be a comparatively simple modification that would result in a more accurate model.

It was assumed that the spacecraft's power systems were 100% efficient. This includes the flywheel energy storage system as well as power conversion and distribution systems. In reality, there would always be losses. Anyone who would continue this work should expand the accuracy of the model by including some realistic efficiencies. Such efficiencies may have an effect on the results.

Several other simplifications were made. Another notable simplification was the engine model which was used. Any or all of these simplifications can be replaced with high-fidelity models, in order to improve the accuracy of the results. In order for the results to be applied to practical situations, several steps in increased model fidelity must be made. However, the concept of applying flywheel energy storage to optimal orbital transfers using solar electric propulsion has passed its first test. It appears that some degree of advantage can be obtained by combining these technologies.

APPENDIX A. Numerical Techniques Used For Integration

In Chapter 3 of the text, we discuss the process of solving boundary value problems to get the desired trajectory for each transfer segment. We start by making first approximations for the time of flight and costates, then we propagate the resulting trajectory using an integration scheme. By making small changes to each of the approximations in turn, and integrating the results, we develop an $N \times N$ Jacobian one column at a time. We then use this Jacobian to find the next step in a Newton iteration. Because several Newton steps must be made to find a single solution, each Newton step requires $N + 1$ integrations (one reference, plus an integration for each of the Jacobian's N columns), and we must solve thousands of these problems to propagate a large-scale orbital transfer, there is a need to perform integration of the equations of motion rapidly. Because thousands of orbital segments are calculated for a large-scale orbital transfer, inaccurate calculations will result in a cumulative effect. For this reason, the integrations performed for these trajectories must be very accurate. In order to get accuracies on the order of 10^{-5} , we determined that each boundary value problem must be solved to within 10^{-8} . The most robust code written required integration accuracy of 10^{-16} in order to achieve convergence.

The code used to solve examples used for this thesis was written in MATLAB, and calculations were performed on a 200 MHz Pentium personal computer. MATLAB has built-in routines for integration, including ODE45, which is a fourth and fifth-order Runge-Kutta integrator. ODE45 is not accurate enough for these problems. If ODE45, or any of the other integration schemes included with MATLAB are used to integrate the equations of motion, the boundary value problems will not converge. A higher order

method was needed, and ODE78 was found to correct the problem. ODE78 is a seventh and eighth-order Runge-Kutta integrator, based on the ODE45 code.

APPENDIX B Conversion to and From Canonical Units

The code written to integrate and solve each of the boundary value problems in this text was designed to accept information in canonical units only. This simplifies the code by generalizing each problem. Before this code can be used, a conversion to canonical units must be performed. In order to obtain meaningful results, the results of each transfer segment must be converted to useful units. In this appendix, we describe the canonical unit system, and describe the methods used to convert quantities to and from canonical units.

The canonical system is based on a circular orbit at the spacecraft's initial radius. One distance unit (DU) is equivalent to the orbital radius. One time unit (TU) is the period of time that it takes the spacecraft to trace an arclength of one DU in this circular orbit. One mass unit (MU) is the initial mass of the spacecraft. So, we have defined the conversions for mass, time, and distance, which allow us to make any other necessary conversions. Each of the transfer segments described in this thesis are circle-to-circle transfers, so the initial conditions for radius ($r(0)$) and the radial and transverse components of velocity ($u(0)$ and $v(0)$) are 1 DU, 0 DU/TU, and 1 DU/TU, respectively.

Thrust, mass flow rate, and usable energy storage must be converted to canonical units based on the initial conditions for each transfer segment. When each boundary value problem is solved, a transfer segment is described in canonical units. Because the meanings of the canonical units change with each transfer segment, we do not wait until all of the segments in a large-scale transfer have been solved to convert the results to useful units. Each solved segment is converted to useful units, and the final conditions

become the initial conditions for the next segment, where they form the basis for the next set of canonical units.

Conversions of distance, mass, and velocity are easily performed by using the definitions of the canonical units.

$$\begin{aligned} dist_{can} &= \frac{dist_{norm}}{r(0)} \\ mass_{can} &= \frac{mass_{norm}}{m(0)} \\ vel_{can} &= \frac{vel_{norm}}{v(0)} \end{aligned} \tag{A-1}$$

Here, the subscript *can* is used to denote canonical units, and the subscript *norm* denotes normal units.

An important property of canonical units is the value of the Earth's gravitational parameter μ . We know that:

$$v(0) = \sqrt{\frac{\mu}{r(0)}} \tag{A-2}$$

Solving for μ , we get:

$$\mu = v^2(0)r(0) \tag{A-3}$$

So, $\mu = 1 \text{ DU}^3/\text{TU}^2$.

The calculated definition of a time unit is a bit more complex:

$$\frac{t_{can}}{t_{norm}} = \sqrt{\frac{r^3(0)}{\mu}} \tag{A-4}$$

Because of the presence of μ on the right side of this equation, we do not escape its use entirely.

Using the conversions for time, distance, and mass, we get the following conversions for energy, power, and thrust:

$$\begin{aligned}
 \frac{E_{can}}{E_{norm}} &= \frac{r(0)}{m(0)\mu} \cdot 10^{-6} \\
 \frac{P_{can}}{P_{norm}} &= \frac{10^{-6}}{m(0)} \sqrt{\frac{r^5}{\mu^3}} \\
 \frac{T_{can}}{T_{norm}} &= \frac{r^2(0) \cdot 10^3}{m(0)\mu}
 \end{aligned} \tag{A-5}$$

All of these equations contain a power of ten because of the convention that was used where distances were in kilometers. The energy equation converts from Joules to canonical energy units. Energy storage is usually measured in Watt-hours per kilogram, where 1 Whr/kg = 3600 J. The power and thrust conversion equations convert Watts and Newtons to their respective canonical counterparts.

BIBLIOGRAPHY

1. Alexeev, Yu. A., M. N. Kazeev, and V. A. Pavshuk. "The New Possibilities of Magnetoplasmadynamic Thrusters." Kurchatov Institute, Russian Research Center, Moscow. WWWeb, <http://www.ch70.chel.su/vniitf/events/1994/spe/abstr3.txt>
2. Alfano, S. *Low Thrust Orbit Transfer*. MS Thesis, AFIT/GA/AA/82D-2. School of Engineering, Air Force Institute of Technology (AU), Wright-Patterson AFB OH, December 1982 (AD-A156076).
3. Argonne National Laboratory. "Flywheel Storage For Locomotives." WWWeb, <http://www.anl.gov/LabDB/Current/Ext/H695-text.001.html>.
4. Avila, Edward R. "Parametric Studies and Orbital Analysis For an Electric Orbit Transfer Vehicle Space Flight Demonstration," *Proceedings of the 3rd Annual AAS/AIAA Spaceflight Mechanics Meeting*. 1215-1240. San Diego: Univelt, Inc., 1993.
5. Bowman, W. Jerry and others. *Nonchemical Propulsion* (Second Edition). AFIT textbook, 1994.
6. Cass, John R. *Discontinuous Low Thrust Orbit Transfer*. MS Thesis, AFIT/GA/AA/83D-1. School of Engineering, Air Force Institute of Technology (AU), Wright-Patterson AFB OH, December 1983 (AD-A136908).
7. Christopher, David A. and Raymond Beach. "Flywheel Technology Development Program for Aerospace Applications." *Proceedings of the IEEE 1997 National Aerospace and Electronics Conference NAECON 1997*. 602-608. New York: IEEE Press, 1997.
8. Edwards, John, J. W. Aldrich, David A. Christopher, and Raymond F. Beach. "Flight Test Demonstration of a flywheel Energy Storage System on the International Space Station." *Proceedings of the IEEE 1997 National Aerospace and Electronics Conference NAECON 1997*. 617-621. New York: IEEE Press, 1997.
9. Federal Transit Administration. "Advanced Technology Transit Bus." WWWeb, <http://www.fta.dot.gov/library/technology/attbnet2.htm>
10. Fitzgerald, Alissa M. "Impact of Energy Storage System Mass on the Performance of Orbit Transfer Vehicles Using Solar Electric Propulsion." *Proceedings of the 29th Intersociety Energy Conversion Engineering Conference - IECEC '94*. 316-319. Washington, District of Columbia: IEEE, 1995.

11. Kennedy, F. and M. Jacox. "The Integrated Solar Upper Stage (ISUS) Program." *AIAA 1995 Space Programs and Technologies Conference*. Washington, District of Columbia: AIAA, 1995.
12. Larson, Wiley J. and James R. Wertz. *Space Mission Analysis and Design*. Torrance: Microcosm, Inc., 1992.
13. Miller, T. M., G. B. Seaworth, R. S. Bell, and E. C. Cady. "System-Level Requirements for an Operational solar Electric Orbital Transfer Vehicle." *30th AIAA/ASME/SAE/ASEE Joint Propulsion Conference*. Washington, District of Columbia: AIAA, 1994.
14. McCann *Optimal Launch Time for a Discontinuous Low Thrust Orbit Transfer*. MS thesis, AFIT/GA/AA/88D-7. School of Engineering, Air force Institute of Technology (AU), Wright-Patterson AFB OH, December 1988 (AD-A202693).
15. Pieronek, Thomas J., D. Kent Decker, and Victor A. Spector. "Spacecraft Flywheel Systems - Benefits and Issues." *Proceedings of the IEEE 1997 National Aerospace and Electronics Conference NAECON 1997*. 589-593. New York: IEEE Press, 1997.
16. Rose, M. F. "Space Power Technology." *Conference Record of the 1996 Twenty-Second International Power Modulator Symposium*. 9-14. New York: IEEE Press, 1996.
17. Rosen Motors. "Technical Description of the Rosen Motors hybrid Electric Powertrain." WWWeb, <http://www.rosenmotors.com/techdesc.htm>
18. Santo, G. Espiritu; S. P. Gill, J. F. Kotas, and R. Paschall. *Feasibility of Flywheel Energy Storage Systems for Applications in Future Space Missions*. NASA Contract NAS3-25808. Caroga Park CA: Rockwell International, Rocketdyne Division. Prepared for Lewis Research Center. January 1995.
19. Scheel, Wayne A. and Bruce A. Conway. "Optimization of Very-Low-Thrust, Many-Revolution Spacecraft Trajectories." *Journal of Guidance, Control, and Dynamics*. 17(6): 1185-1192 (1994).
20. Spencer, David B., and Robert D. Culp. "Designing Continuous-Thrust Low-Earth-Orbit to Geosynchronous-Earth-Orbit Transfers." *Journal of Spacecraft and Rockets*. 32(6): 1033-1038 (1995).
21. Szabo, James. "Solar Electric Propulsion Systems." 21 November 1995. WWWeb, <http://www.afbmd.laafb.af.mil/xrt/xrts/spclft/tnprop8.htm>
22. Thorne, James D. *Optimal Continuous-Thrust Orbit Transfers*. AFIT/DS/ENY/96-7. School of Engineering, Air Force Institute of Technology (AU), Wright-Patterson AFB OH, June 1996 (No DTIC entry).

23. Thorne, James D. and Chris D. Hall. "Approximate Initial Lagrange Costates for Continuous-Thrust Spacecraft," *Journal of Guidance, Control and Dynamics*. 19(2): 283-288 (1996).

24. Wiesel, William E. *Spaceflight Dynamics*. New York: McGraw-Hill, 1989.

Vita

Captain Mark W. Marasch was born on 15 August 1969, in Poughkeepsie, New York. He graduated from Boulder High School in 1988 and entered undergraduate studies and Air Force ROTC at the University of Colorado, Boulder. He graduated with a Bachelor of Science degree in Aerospace Engineering on 15 May 1992. He was commissioned as an Air Force Second Lieutenant the same day.

His first assignment was at Wright-Patterson AFB as a project engineer working on the AC-130U Gunship. His second assignment was as a Fighter Flying Qualities Analyst at the National Air Intelligence Center. During these two assignments, he met and married Catherine D. Schantz, a pension analyst and an Ohio native.

In May 1996, he entered a masters degree program at the Air Force Institute of Technology (AFIT) Graduate School of Engineering, Department of Aeronautics and Astronautics, where he majored in Astronautical Engineering. After graduation in December 1997, Captain Marasch's follow-on assignment was to Phillips Laboratory at Kirtland AFB, New Mexico.

Permanent Address: 144 Sentinel Rock Lane
Boulder, CO 80302